J. Fluid Mech. (2004), *vol.* 499, *pp.* 111–138.
DOI: 10.1017/S0022112003007031 Printed in the United Kingdom

Scattering of incident disturbances by an annular cascade in a swirling flow

By H. M. ATASSI[1], A. A. ALI[1], O. V. ATASSI[2] AND I. V. VINOGRADOV[1]

[1]University of Notre Dame, Notre Dame, IN 46556, USA

[2]Pratt & Whitney, East Hartford, CT 06108, USA

(Received 23 September 2002 and in revised form 9 July 2003)

Analytical and numerical analyses are developed for the interaction and scattering of incident acoustic and vortical disturbances by an unloaded annular cascade in a swirling flow. The mathematical formulation uses the Euler equations linearized about an axial and swirling mean flow. The incident disturbances are decomposed into nearly sonic and nearly convected disturbances using the results of a normal-mode analysis, namely the unsteady pressure is predominantly associated with the former. Exact non-reflecting inflow/outflow conditions are derived in terms of the normal modes using the group velocity to segregate the modes propagating downstream and upstream. An inflow condition is also derived for the nearly convected disturbances. An explicit primitive-variable scheme is implemented and validated by comparison with the uniform flow and narrow annulus limits. Acoustic and aerodynamic results are presented to examine how swirl modifies the scattering from that of the uniform flow and narrow annulus limits and to determine the conditions leading to strong scattering. The results indicate that the swirl changes the physics of the scattering in three major ways: (i) it modifies the number of acoustic modes in the duct, (ii) it changes their duct radial profile, and (iii) it causes significant amplitude and radial phase variations of the incident disturbance. The results also show that when the radial phase of the incident disturbance is different from that of the duct modes, weak scattering into the duct acoustic modes occurs. These results suggest that analysis of the radial variation of the incident disturbance and duct modes can provide an indication of the efficiency of the scattering process.

1. Introduction

The interaction of incident acoustic and vortical disturbances with an annular cascade is an important source of noise and vibration in turbofan engines. The cascade scatters the incident waves into different acoustic and vortical disturbances. The scattering process depends on the cascade geometry and the characteristics of the mean flow and incident disturbances. Downstream of a fan and upstream of the guide vanes, the flow is not uniform but has a swirling motion. The swirl is produced by the work done on the flow by the fan. In an inviscid model of the flow through a rotor or a stator row, the resulting swirl is potential with vortex sheets extending downstream of the blades. In a real flow, blade wake defects, tip and hub vortices, flow separation and turbulent mixing produce significant vorticity in the flow, which may be initially confined to local regions that are separated by potential flow. However, in a rotor/stator stage, time-averaging for large-scale periodic disturbances is equivalent

to averaging in the azimuthal direction, θ. As a result, the mean swirl is rotational. The swirl produces centrifugal and Coriolis forces resulting in a force imbalance that deflects the fluid motion and couples the acoustic, entropic and vortical modes (Kerrobrock 1977). The present paper examines the effect of mean flow swirl on the acoustic and aerodynamic response of an annular cascade.

A simple model for the scattering problem is the two-dimensional cascade which is obtained by unrolling the annular cascade into an infinite linear cascade. This approximation is valid in the limit where the annulus gap between the tip and hub radii is small compared to the average radius. In this case, the centrifugal forces resulting from the swirling motion may be neglected and the upstream mean flow may be considered to be uniform and two-dimensional.

For a flat-plate linear cascade in a uniform flow, the unsteady velocity field can be split into purely convected incident vortical disturbances and scattered potential disturbances. These disturbances are only coupled by the impermeability condition along the blade surface. The linearized governing equations of the scattered field have constant coefficients and thus the problem can be formulated in terms of a singular integral equation (Kaji & Okazaki 1970*b*; Goldstein 1976; Atassi 1994). Numerical solutions have been obtained for the unsteady pressure distribution on the blades and the acoustic radiation upstream and downstream (Kaji & Okazaki 1970*a*; Smith 1971; Atassi & Hamad 1981). More recently, analytical formulations using the Wiener–Hopf method were developed for the linear-cascade aerodynamic and acoustic fields (Peake & Kerschen 1995; Glegg 1999).

For a loaded linear cascade in an inviscid potential flow, the velocity field can still be split into vortical and potential disturbances. However, as for the case of a single airfoil, the vortical disturbances are no longer purely convected but undergo significant distortion as they are carried downstream by the mean flow (Goldstein & Atassi 1976). The potential disturbances are governed by an inhomogeneous non-constant-coefficient convected wave equation (Goldstein 1978). The singular behaviour at the stagnation point can be removed by modifying the splitting to make it suitable for numerical calculations (Atassi & Grzedzinski 1989). This modified splitting was implemented for the problem of a single airfoil in a gust in Scott & Atassi (1995), and for a cascade of airfoils in Hall & Verdon (1991) and Fang & Atassi (1993).

The three-dimensional geometry of the annular duct was first considered by Schulten (1982) and Namba (1987) for a zero-stagger cascade using a singularity method. Their model accounts correctly for the duct acoustic modes. However, such methods cannot be extended to staggered and/or loaded cascades since they cannot account for the effects of non-uniform mean flow.

A linearized Euler analysis was developed by Montgomery & Verdon (1997). At the inlet, they assumed that the gust was convected by the mean flow, thus neglecting changes in amplitude and phase of the incoming disturbance caused by the mean flow. Golubev & Atassi (2000*b*) and Elhadidi *et al.* (2000) showed that these changes significantly modified the evolution of the unsteady incident vortical disturbances. More recently, Podboy *et al.* (2002) presented measurements that show significant effect of the swirl on wake evolution. Golubev & Atassi (2000*a*) developed a model for the interaction of unsteady incident disturbances in a swirling mean motion with an annular cascade of unloaded blades. The incident disturbances are modelled using a combined normal-mode analysis with initial-value problem solutions. Numerical solutions were obtained only for the unsteady blade pressure.

In the present paper, analytical and numerical analyses are developed for the interaction of incident disturbances propagating in a mean swirling flow with an

unloaded annular cascade. The objective of the paper is (i) to develop a basic understanding of how swirl changes the physics of the scattering of both acoustic and vortical disturbances and (ii) to determine the conditions that result in strong scattering. The paper will also provide an accurate and efficient numerical scheme for the calculation of blade unsteady forces and the upstream and downstream radiated sound.

As a first step and because of the coupling between pressure, vorticity, and entropy modes, an analysis will be developed for the representation of upstream disturbances in swirling mean flows. The need for such analysis arises from the fact that the upstream flow is not uniform and for subsonic flows some information has to come from the solution inside the computational domain. As a result, upstream disturbances cannot be specified arbitrarily. The incident upstream disturbance should not have any component that propagates opposite to the flow direction. Consequently, an exact analytical representation of the upstream disturbance requires *a priori* knowledge of how to separate disturbances into inflow and outflow components. For a uniform flow, this is available since the pressure, vorticity, and entropy are uncoupled. For a swirling mean flow, the representation of upstream disturbances will be based on the normal-mode analysis (Golubev & Atassi 1998; Ali, Atassi & Atassi 2000; Ali 2001). This analysis shows that mean swirl may significantly modify the acoustic and vortical spectral composition of the propagating modes in the duct. The analysis also shows that vortical nearly convected modes have very small pressure content. However, significant vorticity may be associated with the acoustic modes, if the mean flow is rotational.

Another important step in the formulation and implementation of the scattering problem is the derivation of non-reflecting boundary conditions. The authors (Ali, Atassi & Atassi 2001) have previously derived non-reflecting boundary conditions for 'acoustic' and 'vortical' waves propagating in a duct with swirling flow. These boundary conditions have been implemented in an explicit scheme and tested by computing the propagation of 'acoustic' and 'vorticity' waves and comparing the solutions with the normal-mode analysis. These solutions have also been validated in Atassi & Ali (2002) for the scattering of vortical waves by an annular cascade in a uniform flow by comparison with the integral solutions of Namba & Schulten (2000).

In § 2 the mathematical formulation is presented and a condition for the incident nearly convected disturbances is derived. In § 3 the inflow/outflow non-reflecting boundary conditions are presented. In § 4 numerical results are presented, and compared with those of the uniform flow and the narrow annulus limits, to show how swirl modifies the scattering phenomena and what conditions result in strong scattering of the incident field.

2. Mathematical formulation

We consider the flow downstream of a fan rotating with an angular velocity Ω. Such a flow is characterized by non-uniformities caused by blade wake defects and tip and hub vortices, flow separation and turbulent mixing. In addition, the flow has a swirling motion created by the loaded blades of the fan. Downstream of the fan, there is an annular cascade of guide vanes as shown schematically in figure 1. The mean flow through the cascade is non-uniform and swirling. For simplicity, we consider thin blades curved along the steady streamlines. We assume that the flow quantities are given at an axial cross-section, $x = x_i$, downstream of which viscous and heat-conducting effects are negligible. We use the Euler equations as the governing

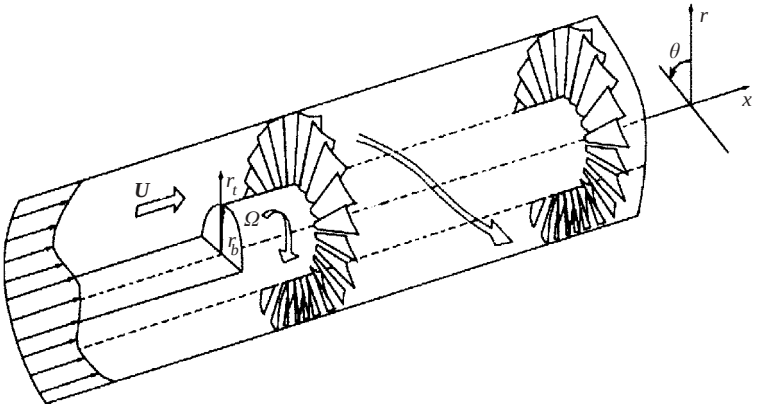

FIGURE 1. Schematic of an annular cascade in a swirling flow. Downstream of the fan, the mean flow is swirling and the wakes shed by the fan blades interact with an annular cascade of guide vanes. Note that the guide vanes are curved along the mean streamlines.

equations and expand the flow quantities as follows:

$$\boldsymbol{U}(\boldsymbol{x}, t) = \boldsymbol{U}(\boldsymbol{x}) + \boldsymbol{u}(\boldsymbol{x}, t), \tag{2.1}$$

$$p(\boldsymbol{x}, t) = p_0(\boldsymbol{x}) + p'(\boldsymbol{x}, t), \tag{2.2}$$

$$\rho(\boldsymbol{x}, t) = \rho_0(\boldsymbol{x}) + \rho'(\boldsymbol{x}, t), \tag{2.3}$$

where $\boldsymbol{x}$ stands for the position vector, t for time, and $\boldsymbol{U}, p_0, \rho_0$ are the steady mean velocity, pressure, and density, respectively. The corresponding unsteady perturbation quantities, $\boldsymbol{u}$, p', ρ' are such that $|\boldsymbol{u}(\boldsymbol{x}, t)| \ll |\boldsymbol{U}(\boldsymbol{x})|$, $|p'(\boldsymbol{x}, t)| \ll p_0(\boldsymbol{x})$ and $|\rho'(\boldsymbol{x}, t)| \ll \rho_0(\boldsymbol{x})$.

Because of the rotational motion of the fan and that of the flow, time averaging for the large-scale periodic disturbances is essentially equivalent to averaging in the azimuthal direction θ. As a result, the mean swirling flow $\boldsymbol{U}(\boldsymbol{x})$ is, in general, vortical and can be assumed to be axisymmetric, of the form

$$\boldsymbol{U}(\boldsymbol{x}) = U_x(r)\boldsymbol{e}_x + U_\theta(r)\boldsymbol{e}_\theta, \tag{2.4}$$

where U_x and U_θ are the mean velocity components in the axial and circumferential directions, respectively; $\boldsymbol{e}_x$ and $\boldsymbol{e}_\theta$ represent unit vectors in the axial and circumferential directions, respectively.

We further assume the flow to be isentropic and non-dimensionalize all lengths with respect to the mean radius r_m, all velocities with respect to the speed of sound c_{om}, and the density by ρ_{0m}, where the subscript m refers to conditions at r_m.

We assume time-harmonic disturbances of the form $\mathrm{e}^{-\mathrm{i}\omega t}$ and define the reduced frequency as $\tilde{\omega} = \omega r_m / c_{om}$. Since the numerical scheme used for our computations is explicit, we retain the time-derivative terms in the equations with the understanding that they will vanish for large time. The linearized Euler equations can be written as follows:

$$\left([I] \left(\frac{\partial}{\partial t} - \mathrm{i}\omega \right) + [A_x] \frac{\partial}{\partial x} + [B_\theta] \frac{1}{r} \frac{\partial}{\partial \theta} + [C_r] \frac{\partial}{\partial r} + [D] \right) \boldsymbol{Y} = 0, \tag{2.5}$$

where

$$\boldsymbol{Y} = \begin{bmatrix} \rho' \\ u_x \\ u_\theta \\ u_r \end{bmatrix}, \tag{2.6}$$

$$[A_x] = \begin{bmatrix} U_x & \rho_0 & 0 & 0 \\ c_0^2/\rho_0 & U_x & 0 & 0 \\ 0 & 0 & U_x & 0 \\ 0 & 0 & 0 & U_x \end{bmatrix}, \tag{2.7}$$

$$[B_\theta] = \begin{bmatrix} U_\theta & 0 & \rho_0 & 0 \\ 0 & U_\theta & 0 & 0 \\ c_0^2/\rho_0 & 0 & U_\theta & 0 \\ 0 & 0 & 0 & U_\theta \end{bmatrix}, \tag{2.8}$$

$$[C_r] = \begin{bmatrix} 0 & 0 & 0 & \rho_0 \\ 0 & 0 & 0 & 0 \\ 0 & 0 & 0 & 0 \\ c_0^2/\rho_0 & 0 & 0 & 0 \end{bmatrix}, \tag{2.9}$$

and

$$[D] = \begin{bmatrix} 0 & 0 & 0 & \mathrm{d}\rho_0/\mathrm{d}r + \rho_0/r \\ 0 & 0 & 0 & \mathrm{d}U_x/\mathrm{d}r \\ 0 & 0 & 0 & U_\theta/r + \mathrm{d}U_\theta/\mathrm{d}r \\ (\mathrm{d}/\mathrm{d}r)(c_0^2/\rho_0) & 0 & -2U_\theta/r & 0 \end{bmatrix}, \tag{2.10}$$

where $[I]$ is the unit matrix and u_x, u_r and u_θ are the components of the disturbance velocity $\boldsymbol{u}$ in the axial, radial and circumferential directions, respectively. Since the flow is isentropic, the unsteady pressure is related to the unsteady density by $p' = c_0^2\rho'$.

We take the origin of the x-axis at the blade midchord at the mean radius. The blades are placed along the mean-flow stream surfaces,

$$\theta - \frac{xU_\theta}{rU_x} = \frac{2\pi\nu}{V}, \quad \nu = 0, 1, \cdots V - 1, \tag{2.11}$$

where V is the number of blades of the annular cascade. Equations (2.5) are solved for an incoming upstream disturbance using the Lax–Wendroff scheme in a single blade passage bounded by the mean-flow stream surfaces defined by (2.11). The blades are placed in the middle of the computational domain along these stream surfaces. Computations are performed using the curvilinear coordinates,

$$\xi = x, \tag{2.12}$$

$$\eta = r, \tag{2.13}$$

$$\zeta = \theta - \frac{xU_\theta}{rU_x}. \tag{2.14}$$

Note that the computational coordinate system is non-orthogonal and that for the existing solution to the Euler equations the scheme maintains second-order accuracy.

Non-reflecting boundary conditions are imposed at the duct inlet and exit. These boundary conditions, explained briefly below, were derived and tested for acoustic and

vortical disturbances in Ali *et al.* (2001) and Atassi & Ali (2002). The impermeability condition is imposed at the hub and tip radii and on the blade surfaces.

2.1. *Incident disturbance representation*

In a scattering problem, the upstream disturbances are the sum of incident and scattered disturbances, i.e.

$$\boldsymbol{u} = \boldsymbol{u}_i + \boldsymbol{u}_s, \tag{2.15}$$

$$p' = p'_i + p'_s, \tag{2.16}$$

where the subscripts i and s denote the incident and scattered disturbances, respectively. The incident disturbances are specified while the scattered disturbances are obtained from the solution of the problem. For a uniform upstream flow, it is always possible to split an incident isentropic field into acoustic and vortical modes (Kovasznay 1953; Atassi 1994),

$$\boldsymbol{u}_i = \boldsymbol{u}^{(a)} + \boldsymbol{u}^{(v)}. \tag{2.17}$$

The incident acoustic waves must satisfy the governing equations and can be expressed in terms of the acoustic modes. The vortical disturbances are purely convected and can be arbitrarily specified but must be solenoidal to satisfy the continuity equation. Since the pressure is entirely associated with the acoustic modes, $p'_i = p'^{(a)}$, the acoustic velocity, $\boldsymbol{u}^{(a)}$, can be expressed in terms of the pressure modes $p'^{(a)}$. Thus by specifying the incident field $\{\boldsymbol{u}_i, p'_i\}$, both $\boldsymbol{u}^{(a)}$ and $\boldsymbol{u}^{(v)}$ are known.

For an upstream swirling flow, the normal-mode analysis shows that the incident disturbances can still be considered as the sum of nearly sonic modes and vorticity-dominated nearly convected modes,

$$\boldsymbol{u}_i = \boldsymbol{u}^{(a)} + \boldsymbol{u}^{(v)}, \tag{2.18}$$

$$p'_i = p'^{(a)} + p'^{(v)}. \tag{2.19}$$

However, the pressure associated with the nearly convected modes $p'^{(v)}$ is very small and may be neglected. Thus $p'_i \sim p'^{(a)}$. It is shown in the Appendix that, as for a uniform flow, $\boldsymbol{u}^{(a)}$ can be expressed in terms of the pressure modes $p'^{(a)}$, where each modal velocity can be entirely expressed in terms of the corresponding modal pressure. Thus, as for the case of a uniform flow, by specifying the incident field $\{\boldsymbol{u}_i, p'_i\}$, we can determine both $\boldsymbol{u}^{(a)}$ and $\boldsymbol{u}^{(v)}$. For the scattered field, $\boldsymbol{u}_s = \boldsymbol{u} - \boldsymbol{u}_i$, an inflow non-reflecting boundary condition must be applied. Similarly, at the exit location the pressure associated with the nearly convected modes, $p'^{(v)}$, is neglected and we apply a non-reflecting boundary condition on the total unsteady pressure p'. This will complete the formulation of the scattering boundary value problem.

We now examine the upstream condition which must be satisfied by the vortical velocity $\boldsymbol{u}^{(v)}$. We first note that since both $\boldsymbol{u}_i$ and $\boldsymbol{u}^{(a)}$ satisfy the linear equations (2.5), $\boldsymbol{u}^{(v)} = \boldsymbol{u}_i - \boldsymbol{u}^{(a)}$ must also satisfy (2.5). However, in practice it is desirable to formulate the upstream incident disturbances in terms of flow quantities in a given cross-section, $x = x_i$. The continuity and the x-momentum equations can be rewritten in the form

$$\nabla \cdot \left(\rho_0 \boldsymbol{u}^{(v)}\right) = -\frac{\mathrm{D}_0 \rho'^{(v)}}{\mathrm{D}t}, \tag{2.20}$$

$$\frac{\mathrm{D}_0 u_x^{(v)}}{\mathrm{D}t} + u_r^{(v)} \frac{\mathrm{d}U_x}{\mathrm{d}r} = -\frac{1}{\rho_0} \frac{\partial p'^{(v)}}{\partial x}, \tag{2.21}$$

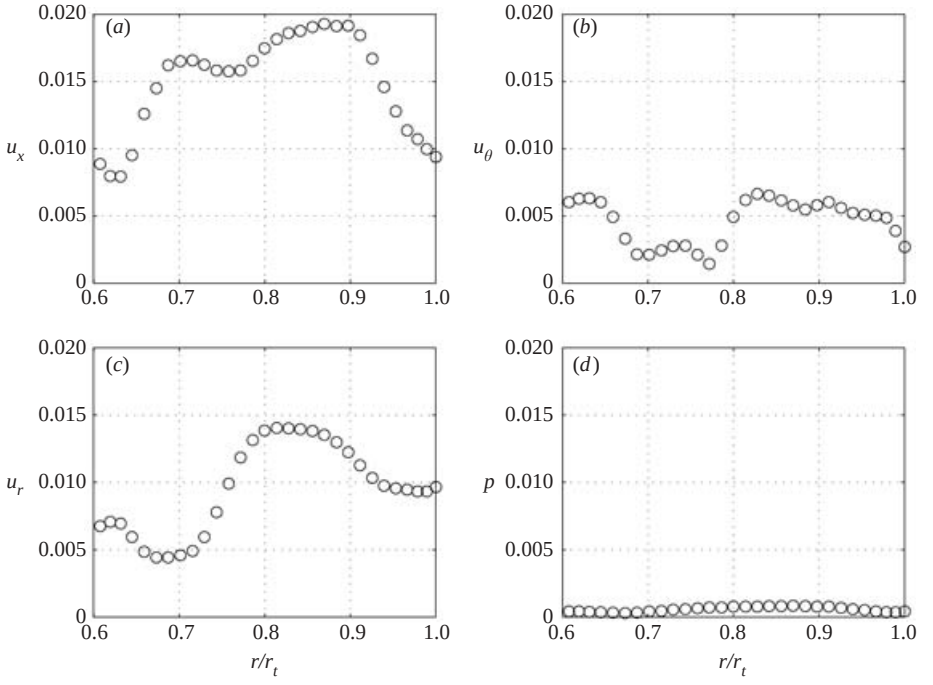

FIGURE 2. The non-dimensional velocity and pressure of the first harmonic of a typical fan wake. The velocity is non-dimensionalized by the speed of sound at the mean radius, c_{0m}, and the pressure is non-dimensionalized by $\rho_{0m}c_{0m}^2$, where ρ_{0m} is the density at the mean radius. (*a*) Axial velocity, (*b*) circumferential velocity, (*c*) radial velocity and (*d*) pressure. Note that the first-harmonic pressure field associated with the wake is small compared to the first-harmonic velocity component of the wake.

where

$$\frac{\mathrm{D}_0}{\mathrm{D}t} \equiv \frac{\partial}{\partial t} + \boldsymbol{U}(\boldsymbol{x})\cdot\nabla. \tag{2.22}$$

Eliminating $\partial u_x/\partial x$, we obtain,

$$\left(\frac{\partial}{\partial t} + \frac{U_\theta}{r}\frac{\partial}{\partial \theta}\right) u_x^{(v)} - \frac{U_x^2}{r\rho_0}\frac{\partial}{\partial r}\left(\frac{r\rho_0 u_r^{(v)}}{U_x}\right) - \frac{U_x}{r}\frac{\partial u_\theta^{(v)}}{\partial \theta} = -\frac{1}{\rho_0}\left(\frac{\partial p'^{(v)}}{\partial x} - U_x\frac{\mathrm{D}_0\rho'^{(v)}}{\mathrm{D}t}\right). \tag{2.23}$$

The normal-mode analysis (Ali 2001) suggests that for the nearly convected vorticity-dominated modes, $p'^{(v)}$ and $\rho'^{(v)}$ are very small compared to the perturbation velocity, even at low frequencies. These results are also confirmed by RANS calculations of the wakes shed from a fan. The wake has been decomposed into Fourier harmonics and the velocity and pressure of the first wake harmonic are plotted in figure 2. The figure shows that the non-dimensionalized pressure fluctuations are small and appear to scale with the square of those of the velocity. We therefore neglect the right-hand side of (2.23) only at the inlet section, $x = x_i$, and thus obtain the following relation for the incident vortical disturbances at $x = x_i$:

$$\left(\frac{\partial}{\partial t} + \frac{U_\theta}{r}\frac{\partial}{\partial \theta}\right) u_x^{(v)} - \frac{U_x^2}{r\rho_0}\frac{\partial}{\partial r}\left(\frac{r\rho_0 u_r^{(v)}}{U_x}\right) - \frac{U_x}{r}\frac{\partial u_\theta^{(v)}}{\partial \theta} = 0. \tag{2.24}$$

Note that the right-hand-side terms in (2.23) are taken into account in our numerical scheme to avoid error accumulation over the range of integration. Condition (2.24)

reduces in the uniform flow limit to the condition that the incoming gust velocity must be solenoidal. Golubev & Atassi (2000*a*) used a high-frequency approximation to impose a divergence-free condition on the vortical incident velocity. Condition (2.24) reduces to the divergence-free condition in the high-frequency limit.

Without loss of generality, we can expand the vortical velocity in terms of a Fourier series,

$$\boldsymbol{u}^{(v)} = \sum_{m_g=-\infty}^{m_g=+\infty} \hat{\boldsymbol{u}}_{m_g}(x_i, r)\, \mathrm{e}^{\mathrm{i}(m_g\theta-\omega t)}. \tag{2.25}$$

Considering one Fourier component $\hat{\boldsymbol{u}}_{m_g} = \{\hat{u}_{xm_g}, \hat{u}_{rm_g}, \hat{u}_{\theta m_g}\}$ and substituting in the condition (2.24), we obtain

$$\mathrm{i}\alpha\hat{u}_{xm_g} + \frac{\mathrm{i}m_g}{r}\hat{u}_{\theta m_g} + \frac{U_x}{r\rho_0}\frac{\partial}{\partial r}\left(\frac{r\rho_0}{U_x}\hat{u}_{rm_g}\right) = 0, \tag{2.26}$$

where we have put

$$\alpha = \frac{\omega}{U_x} - \frac{m_g U_\theta}{rU_x}. \tag{2.27}$$

Note that the radial velocity $\hat{u}_{rm_g}(r)$ must satisfy the impermeability condition at the hub and the tip.

2.2. *Quasi-periodic condition*

A quasi-periodic condition is applied in the θ-direction:

$$\boldsymbol{Y}(x, \theta_e, r) = \boldsymbol{Y}(x, 0, r)\, \mathrm{e}^{\mathrm{i}\sigma}, \tag{2.28}$$

where $\sigma = m_g\theta_e$, $\theta_e = 2\pi/V$. All flow quantities of the scattered field upstream of the blades must satisfy this condition. This condition must also be applied to the density and the velocity component normal to the wakes downstream of the blades (vanes). Thus the propagating acoustic waves must satisfy the condition

$$m\theta_e = m_g\theta_e - 2q\pi, \tag{2.29}$$

where q is an integer. For a rotor/stator interaction, $m_g = pB$, where B is the number of fan blades, and p is the harmonic index, and hence we arrive at the Tyler & Sofrin (1962) condition

$$m = pB - qV. \tag{2.30}$$

3. Non-reflecting boundary conditions

Away from the blade row, the far-field behaviour of the scattered unsteady disturbances is governed by the normal-mode analysis. As noted above, the unsteady pressure and density are associated with the nearly sonic modes, which are stable propagating or evanescent modes (Golubev & Atassi 1998; Ali *et al.* 2000; Ali 2001) of the form

$$\mathscr{P}_{mn}(r)\mathrm{e}^{\mathrm{i}(k_{mn}x+m\theta-\omega t)}, \tag{3.1}$$

where k_{mn} is the axial wavenumber corresponding to the pressure eigenfunction $\mathscr{P}_{mn}(r)$ and m and n are integers representing the azimuthal and radial mode numbers, respectively. Note that the radial mode number, n, generally represents the number of zero crossings of $\mathscr{P}_{mn}(r)$ between r_h and r_t. For such modes, no complex ω with positive imaginary part is obtained for real k from the dispersion relation. Hence, the group velocity

$$c_g = \frac{\mathrm{d}\omega}{\mathrm{d}k} \tag{3.2}$$

gives the direction of propagation of the waves (Briggs 1964, p. 33). This may not be true for unstable nearly convected modes.

We therefore use the group velocity to segregate the modes propagating downstream (upstream) and denote them with the superscript + (−), respectively. The downstream (upstream) unsteady pressure can then be expressed in terms of the downstream (upstream) propagating modes as follows:

$$p'^{\pm}(x, r, \theta; t) = \int_{-\infty}^{+\infty} \sum_{n=0}^{\infty} \sum_{m \in S_m^{\pm}} c_{mn}^{\pm} \mathscr{P}_{mn}^{\pm}(r)\, \mathrm{e}^{\mathrm{i}(k_{mn}^{\pm} x + m\theta - \omega t)}\, \mathrm{d}\omega, \tag{3.3}$$

where $k_{mn}^{\pm}$ are the axial wavenumbers, $c_{mn}^{\pm}$ are the complex coefficients corresponding to the pressure eigenfunctions $\mathscr{P}_{mn}^{\pm}(r)$, and $S_m^{\pm}$ are the sets of all possible values of m.

In what follows, we consider only one frequency and for computational purposes we truncate the series of equation (3.3) to $\tilde{M}$ circumferential modes and $\tilde{N}$ radial modes,

$$p'^{\pm}(r, \theta, x; t) = \sum_{n=0}^{\tilde{N}} \sum_{m \in \tilde{S}_m^{\pm}} c_{mn}^{\pm} \mathscr{P}_{mn}^{\pm}(r)\, \mathrm{e}^{\mathrm{i}(k_{mn}^{\pm} x + m\theta - \omega t)}, \tag{3.4}$$

where $\tilde{S}_m^{\pm}$ are finite subsets of $S_m^{\pm}$.

Applying expansion (3.4) at two adjacent planes at the boundary, the unknown coefficients c_{mn} can be eliminated yielding a non-reflecting boundary condition.

Numerically, let p'_{ij} be the value of p' at the grid point (i,j) at the exit boundary corresponding to $x = x_N$, where i is the index along the radial direction and j is the index along the circumferential direction,

$$p'_{ij} = \sum_{n=0}^{\tilde{N}} \sum_{m \in \tilde{S}_m^{+}} c_{mn}^{+} \mathscr{P}_{mn}^{+}(r_i)\, \mathrm{e}^{\mathrm{i}(k_{mn}^{+} x_N + m\theta_j - \omega t)}. \tag{3.5}$$

This can be cast in matrix form,

$$\boldsymbol{P}_N = [C_N^+]\boldsymbol{c}, \tag{3.6}$$

where the elements of the vector $\boldsymbol{P}_N$ are the unsteady pressure at the different grid points at the exit plane at $x = x_N$. The elements of the vector $\boldsymbol{c}$ are the coefficients c_{mn}^{+}, and the elements of the matrix $[C_N^+]$ are the values of the normal modes $\mathscr{P}_{mn}^{+}(r_i)\exp[\mathrm{i}(k_{mn}^{+} x_N + m\theta_j)]$ at (i,j).

Similarly, we can write the solution at the previous axial cross-section located at $x = x_{N-1}$ as

$$\boldsymbol{P}_{N-1} = [C_{N-1}^+]\boldsymbol{c}. \tag{3.7}$$

Solving the previous equation for $\boldsymbol{c}$,

$$\boldsymbol{c} = [C_{N-1}^+]^{-1}\boldsymbol{P}_{N-1}, \tag{3.8}$$

and substituting in equation (3.6), we obtain

$$\boldsymbol{P}_N = [C_N^+][C_{N-1}^+]^{-1}\boldsymbol{P}_{N-1}. \tag{3.9}$$

Note that the number of modes used in the expansion may be smaller than the number of grid points of the computational domain. The inversion of the matrix $[C_{N-1}^+]$ in equation (3.9) could be difficult if acoustic modes with very large azimuthal number m are included in the expansion (3.4). Such modes correspond to eigenvalues of very large imaginary part leading to elements of very small values in entire rows

of the matrix $[C^{+}_{N-1}]$ and causing the matrix to be ill conditioned. This problem was addressed by the authors by considering only modes with eigenvalues which do not have large imaginary part.

Equation (3.9) is the exit boundary condition we use to complete the formulation of the boundary-value problem. Note that (3.9) is not local, i.e. the pressure at the point $p'(N, i_0, j_0)$ depends on the value of the pressure at all the grid points of the previous cross-section $(N-1, i, j)$.

The formulation of the inlet condition will be similar to that of the exit condition except that the pressure associated with incoming acoustic waves will be subtracted from the total pressure prior to the application of the inflow conditions,

$$(\boldsymbol{P} - \boldsymbol{P}_i)_1 = [C^{-}_1][C^{-}_2]^{-1}(\boldsymbol{P} - \boldsymbol{P}_i)_2, \tag{3.10}$$

where the elements of the vector $\boldsymbol{P}_i$ represent the pressure of the incident acoustic disturbance, the subscript 1 refers to the axial inlet plane, and the subscript 2 refers to the axial plane adjacent to the inlet plane. The elements of the matrices $[C^{-}_1]$ and $[C^{-}_2]$ in this case correspond to the normal modes propagating upstream and have the eigenfunctions $\mathscr{P}^{-}_{mn}(r_i)$ and the eigenvalues k^{-}_{mn}.

The accuracy of these boundary conditions has been tested for acoustic and vortical propagation in a duct with a swirling flow in Ali *et al.* (2001).

4. Results

In this section, we examine the effects of the various parameters to gain insight into the annular-cascade scattering phenomena. We first consider the uniform flow and narrow annulus limits to validate our results by comparison with those of the lifting surface theories (Namba & Schulten 2000), and linear cascade (Hamad & Atassi 1981). We then present results for a swirling flow in a full annulus to illustrate the new physics which results when the mean flow is non-uniform and swirling. We examine the effects of the cascade three-dimensional geometry, radial swirl distribution, reduced frequency, and incident disturbance characteristics on the unsteady aerodynamic forces and the radiated acoustics. These results are used to establish when the non-uniform swirling flow produces significant changes to the aeroacoustic response and to elicit the conditions that affect the magnitude and nature of the scattered field.

For simplicity, we model the circumferential mean-flow component as a combination of rigid body rotation and potential vortex swirl,

$$U_\theta = \Omega r + \frac{\Gamma}{r}. \tag{4.1}$$

This model is defined by the two constant parameters Ω and Γ. We further assume the flow to be isentropic with a uniform enthalpy from hub to tip. In this case, the axial component of velocity is given by

$$U_x^2 = U_m^2 - 2\left[\Omega^2\left(r^2 - r_m^2\right) + 2\Omega\Gamma\ln(r/r_m)\right], \tag{4.2}$$

where U_m is the axial velocity at the mean radius of the duct r_m. It is convenient for presenting the numerical results to define the axial and swirl velocities in terms of the Mach numbers at the mean radius $M_0 = U_m/c_{om}$, $M_\Omega = (\Omega r_m)/c_{om}$ and $M_\Gamma = \Gamma/(r_m c_{om})$.

We consider the scattering of both incident vortical and acoustic waves. For vortical waves, we take one Fourier component of (2.25),

$$\hat{\boldsymbol{u}}_{m_g} = \hat{u}_{xm_g}\boldsymbol{e}_x + \hat{u}_{rm_g}\boldsymbol{e}_r + \hat{u}_{\theta m_g}\boldsymbol{e}_\theta. \tag{4.3}$$

To facilitate comparison with two-dimensional theory, it is convenient to introduce the upwash velocity component normal to the streamlines in the (x, θ)-plane,

$$a^{(u)}_{m_g}(r) = \frac{-\hat{u}_{xm_g} U_\theta + \hat{u}_{\theta m_g} U_x}{U}, \tag{4.4}$$

where $U = \sqrt{U_x^2 + U_\theta^2}$. Using (2.26) and (4.4) we can then express $\hat{u}_{xm_g}$ and $\hat{u}_{\theta m_g}$ in terms of $\hat{u}_{m_g r}$ and $a^{(u)}_{m_g}(r)$:

$$\hat{u}_{xm_g} = -\frac{m_g a^{(u)}_{m_g} U - \mathrm{i}\dfrac{U_x^2}{\rho_0}\dfrac{\partial}{\partial r}\left(\dfrac{r\rho_0}{U_x}\hat{u}_{rm_g}\right)}{\alpha r U_x + m_g U_\theta}, \tag{4.5}$$

$$\hat{u}_{\theta m_g} = \frac{a^{(u)}_{m_g}\alpha r U + \mathrm{i}\dfrac{U_x U_\theta}{\rho_0}\dfrac{\partial}{\partial r}\left(\dfrac{r\rho_0}{U_x}\hat{u}_{rm_g}\right)}{\alpha r U_x + m_g U_\theta}. \tag{4.6}$$

Incident acoustic waves are expanded in terms of the normal modes as shown in the Appendix . The mn component of the incident pressure is of the form

$$p'_{mn} = c^{(i)}_{mn}\mathscr{P}_{mn}(r)\,\mathrm{e}^{\mathrm{i}(k_{mn}x + m\theta - \omega t)}, \tag{4.7}$$

where $c^{(i)}_{mn}$ is a constant. The upwash for the acoustic mode is defined as

$$a^{(u)}_{mn} = c^{(i)}_{mn}\frac{-u_{xmn}U_\theta + u_{\theta mn}U_x}{U}, \tag{4.8}$$

where u_{xmn} and $u_{\theta mn}$ are the axial and azimuthal acoustic velocities of the $\{mn\}$ mode, respectively. Their expression in terms of $\mathscr{P}_{mn}$ is given in the Appendix.

We define the sectional lift coefficient as

$$c'_l(r) = \frac{L'}{\rho_0 c a^{(u)} U}, \tag{4.9}$$

where L' is the force per unit span and c is the chord length and where we have dropped the subscript for $a^{(u)}$ so that it could represent either a gust (4.4) or an acoustic wave (4.8). The quantities $\rho_0, c, a^{(u)}$, and U are evaluated at the radial location of the considered section. The acoustic coefficients are calculated so that the maximum values of pressure eigenfunctions are equal to unity and the pressure is normalized by $(\rho_{om} c_{om} a^{(u)}_m)$ where ρ_{om}, c_{om}, and $a^{(u)}_m$ are the values of the mean density, the mean speed of sound, and the upwash at the mean radius, respectively.

The calculations are carried out with the blades placed in the middle third of the computational domain along the bounding stream surfaces. Thus the projection of the blades along the x-axis extends from $-(c/2)\cos\chi_m$ to $+(c/2)\cos\chi_m$ and the inlet and outlet of the computational domain are located at $x = \mp(3c/2)\cos\chi_m$, where $\chi_m = \tan^{-1}(U_\theta/U_x)_m$ is the stagger angle at the mean radius.

4.1. *Scattering in the uniform flow limit*

To validate our results, we first consider the limit where the mean flow is uniform and axial. A benchmark case in this limit was proposed by Hanson (1999) and consists of an annular cascade of 24 flat-plate stator vanes placed in an annular duct.

A gust is introduced at the inlet of the duct,

$$\hat{u}_\theta(r) = 0.1U\exp[\mathrm{i}(pB\Omega x/U + 2\pi n_g(r - r_h)/(r_t - r_h))], \tag{4.10}$$

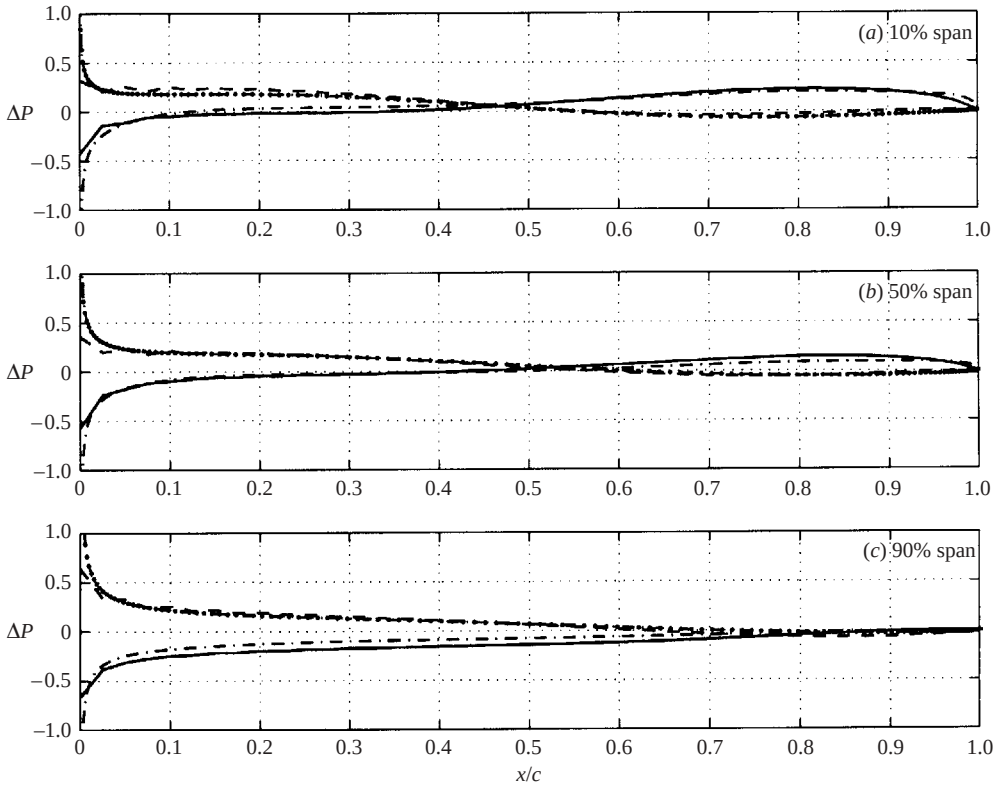

FIGURE 3. Unsteady pressure jump along the blade chord for $n_g = 0$ at different spanwise locations. The present computations (——, real part; – – –, imaginary part) are compared to those of Schulten (— · — ·, real part; · · · · ·, imaginary part).

where U is the axial flow speed, Ω is the rotor angular velocity, $B = 16$ is the number of rotor blades, and n_g is an integer. The blade passing frequency (BPF) fundamental, $p = 1$, was considered. The reduced frequency $\tilde{\omega} = pB\Omega r_m/c_{om} = 9.396$, the hub–tip ratio is 0.5, $c/r_m = 0.2618$, and the Mach number $M = 0.5$. An interesting aspect of this model problem is that it examines the effect that the radial phase variation of the gust has on the unsteady aerodynamic and aeroacoustic response. For the unsteady parameters chosen above, two propagating acoustic modes exist which are denoted by the number of zero crossings (0 and 1) from hub to tip. By increasing the parameter n_g, the radial-mode order of the gust will increase and it is expected that relatively little of the gust will scatter into the low-order acoustic modes which exist in the duct. We consider two cases with wake phase variations, $n_g = 0$, 2. For comparison with the results given in Namba & Schulten (2000), we take

$$\Delta P = \frac{\Delta p'}{\frac{1}{2}\rho_0 U^2}, \qquad c_l' = \frac{L'}{\frac{1}{2}\rho_0 U a^{(u)} c},$$

where $a^{(u)} = 0.1U$ and $\Delta p'$ is the pressure jump across the blade. We also non-dimensionalize the acoustic pressure defined by (3.3) with respect to $\frac{1}{2}\rho_0 U^2$ and denote the coefficients by c^*_{mn}.

Figure 3 shows the real and imaginary parts of the unsteady pressure jump along the blade chord for $n_g = 0$ at different spanwise locations (10%, 50%, and 90% span). The results are in good agreement with those obtained by Shulten as reported in

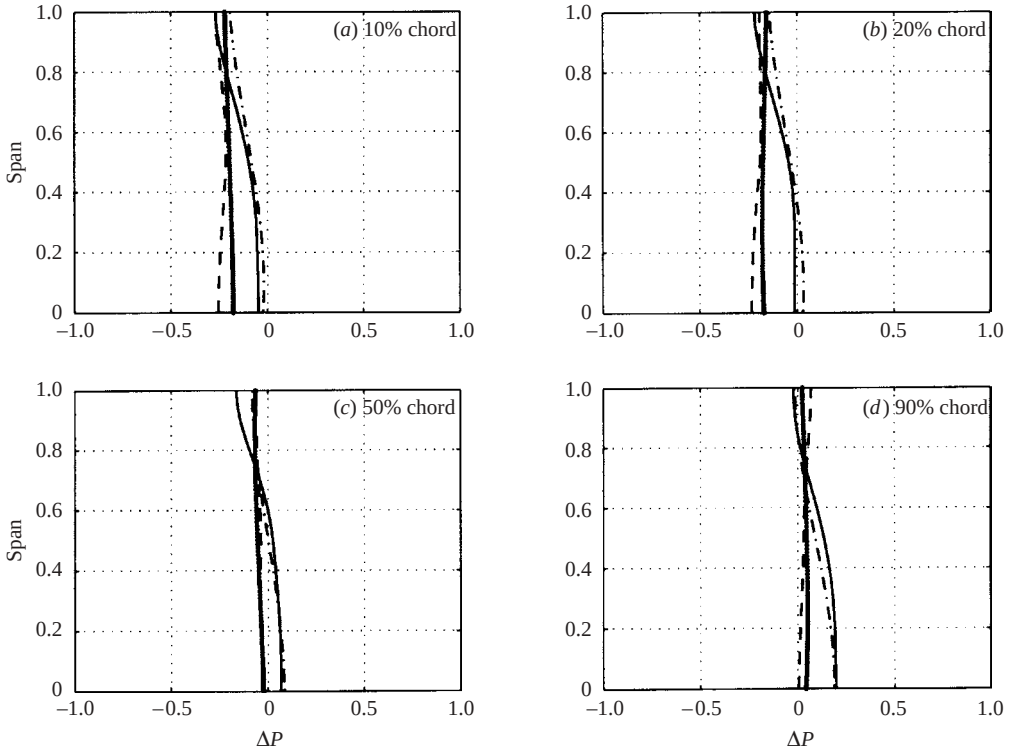

FIGURE 4. Unsteady pressure jump along the blade span for $n_g = 0$ at different chordwise locations. The present computations (——, real part; – – –, imaginary part) are compared to those of Schulten (2000) as reported in Namba & Schulten (2000) (— · — ·, real part; · · · · ·, imaginary part).

Namba & Schulten (2000). Figure 4 shows the real and imaginary parts of the unsteady pressure jump along the blade span for $n_g = 0$ at different chordwise locations (10%, 20%, 50%, and 90% chord). The results agree well with Schulten's results. Slight differences exist at the hub and the tip.

For the acoustic results, the complex coefficients c^*_{mn} are compared to those obtained by Namba & Schulten for the upstream and downstream propagating modes. The normal-mode analysis shows that for the present case, two upstream and two downstream modes $(-8, 0)$ and $(-8, 1)$ exist. The amplitude of the acoustic coefficients, $c^*_{-8,0}$ and $c^*_{-8,1}$, are shown in table 1(*a*) for the upstream propagating modes and in table 1(*b*) for the downstream propagating modes. Note that as we increase n_g from zero to 2 the dominant acoustic response comes from the higher-order acoustic mode. Moreover, as the radial modal number of the gust, n_g, increases, i.e. the number of zero crossings in the wake-defect harmonic increases, less and less of the energy in the gust is able to scatter into the propagating low-order acoustic modes $(-8, 0)$ and $(-8, 1)$. A more detailed comparison of the acoustic results for $n_g = 0, 1, 2, 3$ is given in Atassi & Ali (2002).

4.2. *Scattering in a swirling flow: the narrow annulus limit*

We consider a swirling flow in the narrow annulus limit and compare our three-dimensional annular-cascade computations to those of a linear cascade using the integral formulation given in Atassi & Hamad (1981), for a rotor/stator interaction

	n_g	m	n	Namba	Schulten	Present computations
(a)	0	−8	0	1.1780×10^{-2}	1.1745×10^{-2}	1.1682×10^{-2}
	0	−8	1	1.9301×10^{-2}	1.9064×10^{-2}	1.8518×10^{-2}
	2	−8	0	8.9005×10^{-4}	9.4530×10^{-4}	9.4167×10^{-4}
	2	−8	1	4.8305×10^{-3}	3.8368×10^{-3}	4.0517×10^{-3}
(b)	0	−8	0	1.7144×10^{-2}	1.4972×10^{-2}	1.5020×10^{-2}
	0	−8	1	1.8946×10^{-2}	1.7850×10^{-2}	1.8123×10^{-2}
	2	−8	0	3.3653×10^{-3}	3.0988×10^{-3}	3.1127×10^{-3}
	2	−8	1	6.0722×10^{-3}	6.6977×10^{-3}	6.5683×10^{-3}

TABLE 1. Comparison of the magnitude of (a) the upstream and (b) the downstream acoustic coefficients, $|c^*_{mn}|$, with those obtained by Namba and by Schulten (reported in Namba & Schulten 2000.

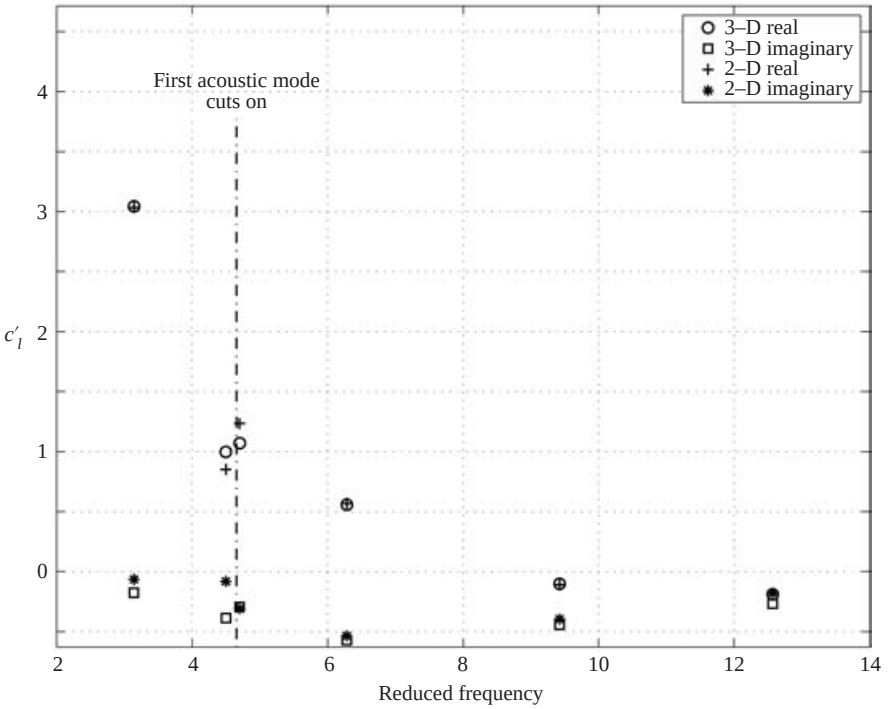

FIGURE 5. Comparison of the real and imaginary parts of the unsteady sectional lift coefficient, c'_l, versus the reduced frequency, $\tilde{\omega}$, between the annular- and linear-cascade calculations in the narrow annulus limit. $M = 0.5$ and stagger $= 45°$.

with $B = 16$ and $V = 24$, a mean-flow total Mach number $M = 0.5$, and a stagger angle of 45° ($M_x = M_\theta = 0.3536$). The non-dimensional chord length, c/r_m, is 0.3491. We consider the BPF fundamental of the gust, i.e. $m_g = B$, and take the gust radial component $\hat{u}_r = 0$. We impose a unit gust upwash amplitude, $a^{(u)} = 1$, and for the annular-cascade calculations, we take $r_h/r_t = 0.98$. The annular-cascade results are compared to those of the linear cascade for reduced frequencies of π, 4.5, 4.7, 2π, 3π, and 4π using a grid of $\{n_x \times n_\theta \times n_r\} = \{81 \times 15 \times 7\}$.

Figure 5 compares the real and imaginary parts of the unsteady lift coefficient for the two cases. The results are generally in good agreement. The maximum differences between the linear and annular cascade calculations occur, as expected, near the first acoustic mode cut-on frequency, $\tilde{\omega} = 4.655$.

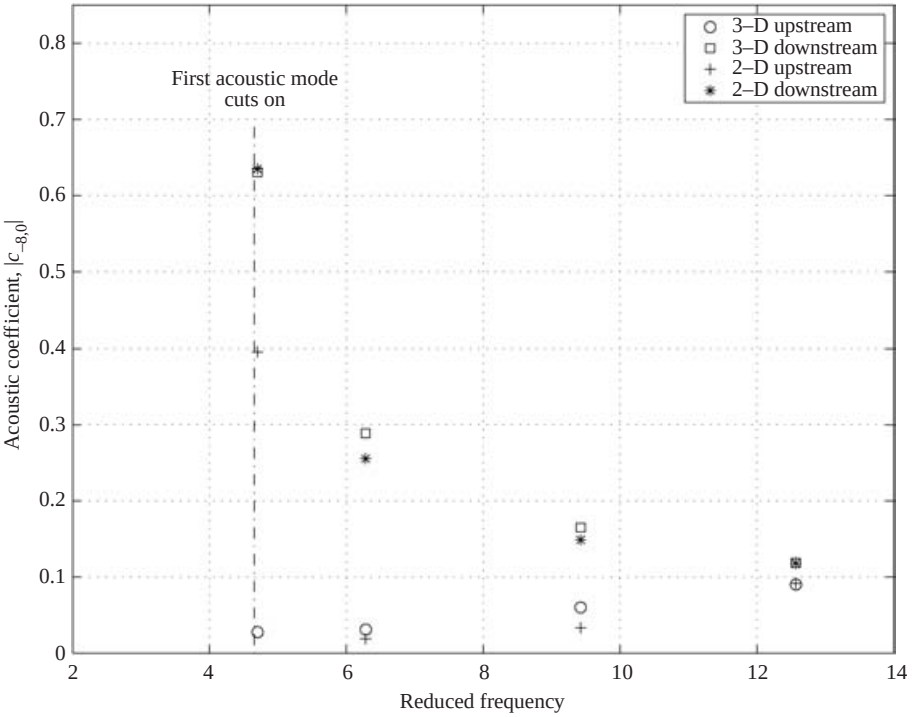

FIGURE 6. Comparison of the upstream and downstream magnitude of the acoustic coefficients, $|c^{\pm}_{-8,0}|$, versus the reduced frequency, $\tilde{\omega}$, between the annular- and linear-cascade calculations in the narrow annulus limit. $M = 0.5$ and stagger $= 45°$.

The magnitude of the upstream and downstream acoustic coefficients obtained from the linear- and annular-cascade calculations are compared in figure 6. In general, the downstream coefficients are in better agreement than the upstream ones. A large difference is observed in the upstream coefficient for $\tilde{\omega} = 4.7$, which is very close to the cut-on frequency; otherwise the agreement between the two cases is good.

4.3. *Scattering in a swirling flow: effect of hub–tip ratio*

As the hub–tip ratio is decreased centrifugal forces, which are neglected by the narrow annulus model, become more important and affect the evolution of the gust. The swirl also causes significant radial variations in the magnitude and phase of the gust. Moreover, it modifies the acoustic duct modes. To study this, we calculate the unsteady lift coefficient and the amplitude of the acoustic modes for the hub–tip ratios 0.6, 0.6667, 0.7391, 0.8182, and 0.9048. Again we take $B = 16$, $V = 24$ and a mean flow of $M_0 = 0.3536$, $M_\Omega = 0.1$, $M_\Gamma = 0.1$. We consider the BPF fundamental of the gust, i.e. $m_g = 16$, and take the gust radial component $\hat{u}_r = 0$. We impose a unit gust upwash amplitude, $a^{(u)} = 1$, at the inlet of the computational domain. The non-dimensional chord at the mean radius is 0.3491, and the reduced frequency $\tilde{\omega} = 3\pi$. For the three cases considered with $r_h/r_t > 0.68$, there is only one propagating acoustic mode. A new acoustic mode cuts on at about $r_h/r_t = 0.68$, and for the other two cases considered with $r_h/r_t < 0.68$, there are two propagating modes.

Figure 7 compares the magnitude of the unsteady sectional lift coefficient $|c_l'|$ along the span for the different hub–tip ratios. The figure shows that for the narrow annulus case, $r_h/r_t = 0.9048$, $|c_l'|$ has, as expected, small variation along the span. As

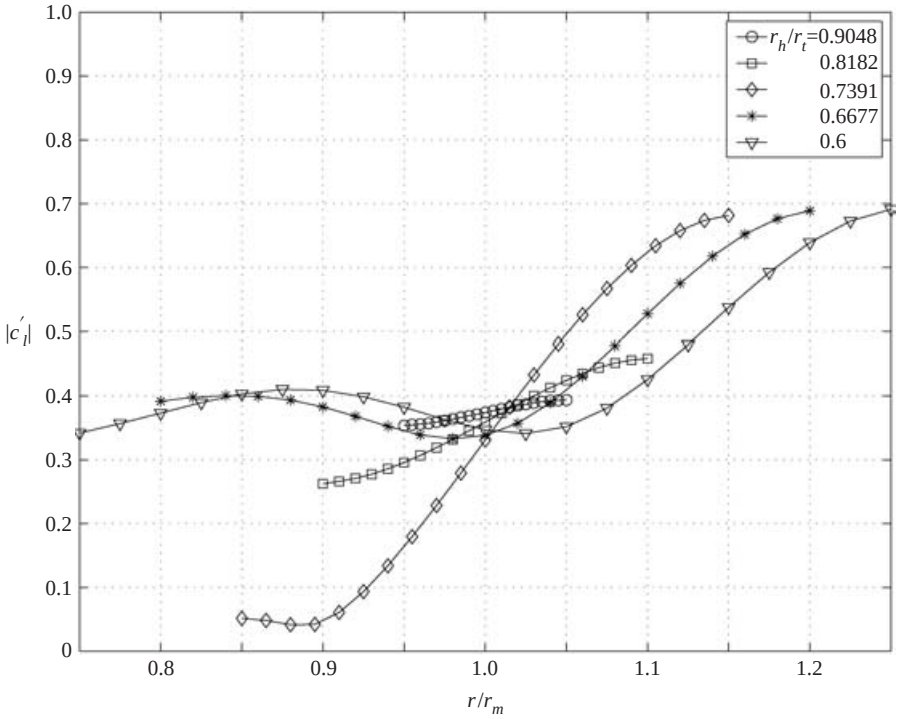

FIGURE 7. Variation of the magnitude of the unsteady sectional lift coefficient, $|c_l'|$, along the span for different hub–tip ratios. A gust upwash amplitude, $a^{(u)} = 1$, is imposed at the inlet of the computational domain. $M_0 = 0.3536$, $M_\Omega = 0.1$, $M_\Gamma = 0.1$, and $\tilde{\omega} = 3\pi$.

this ratio decreases three-dimensional effects become more important and $|c_l'|$ exhibits significant variations. It is interesting to note that for $r_h/r_t = 0.7391$, corresponding to the case where the r_h/r_t gets closer to the value at which a new acoustic mode cuts on, the unsteady sectional lift coefficient has the largest variation along the span. This suggests that in addition to the three-dimensional effects, the aerodynamic and acoustic scattering problem is strongly coupled with the duct acoustics.

The magnitude of the upstream and downstream acoustic coefficients $|c^{\pm}_{-8,\eta}|$ for the different hub–tip ratios are compared in figure 8. The downstream acoustic coefficient of the first radial mode ($n = 0$) decreases slightly as the hub–tip ratio decreases but as the second mode cuts on it starts to increase. Note that the upstream coefficient of the second acoustic mode is substantially higher than that of the first mode, suggesting an increase in the radiated sound. This increase is consistent with the increase in the radial variation of the unsteady pressure on the vane as the hub–tip ratio decreases. These results clearly show that a change in the number of cut-on modes has strong influence on the aerodynamic and acoustic coefficients.

We have mentioned earlier that significant radial variations in the magnitude and phase of the gust occur as it convects in a swirling flow. These variations increase with the distance travelled by the gust before interacting with the vanes. To examine these effects, we calculated the unsteady sectional lift coefficient for the same parameters and conditions except that the gust upwash amplitude, $a^{(u)} = 1$, is imposed at the leading edge of the vanes. This removes most of the radial distortion in the magnitude and phase of the gust as it interacts with the vanes. Figure 9 shows plots of the magnitude of the unsteady sectional lift coefficient $|c_l'|$ along the span for the different

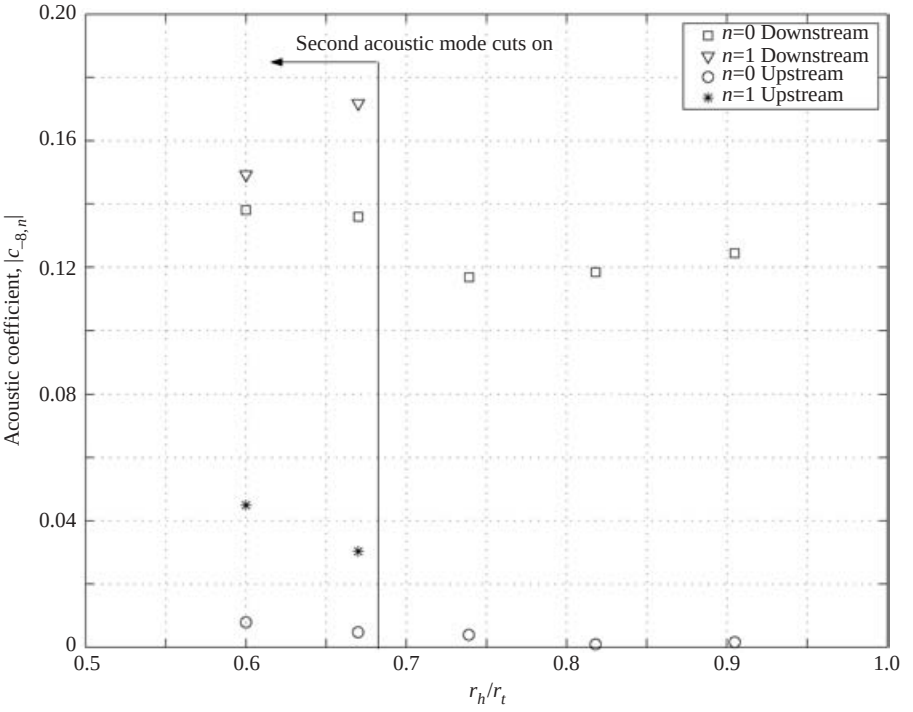

FIGURE 8. Variation of the magnitude of the upstream and downstream acoustic coefficients, $|c^{\pm}_{-8,\eta}|$, along the span for different hub–tip ratios. A gust upwash amplitude, $a^{(u)} = 1$, is imposed at the inlet of the computational domain. $M_0 = 0.3536$, $M_\Omega = 0.1$, $M_\Gamma = 0.1$, and $\tilde{\omega} = 3\pi$.

hub–tip ratios. Comparison of figures 7 and 9 clearly shows the significant effects of the magnitude and phase change of the gust caused by the mean swirl on the aerodynamic response of the cascade. In addition, we note that now the unsteady sectional lift for $r_h/r_t = 0.7391$ has a similar variation pattern as the others. This suggests that an almost uniform vane upwash is less likely to couple with the duct higher-order acoustic modes.

4.4. *Effect of mean-flow variation on the scattering*

Another three-dimensional feature of annular cascades is the radial variation of their mean flows. In what follows, we examine how different radial mean swirl distributions affect the cascade scattering response. We consider four different mean flows with the same total Mach number of 0.4062 at the mean radius. The first mean flow is axial and uniform. The three swirling flows have the same axial and swirl Mach numbers of 0.3536 and 0.2, respectively, at the mean radius and consist of a free-vortex swirl distribution with $M_\Gamma = 0.2$, a rigid-body swirl with $M_\Omega = 0.2$ and a combination of free-vortex and rigid-body swirl, $M_\Gamma = 0.1$ and $M_\Omega = 0.1$. The geometry and frequency parameters are $c/r_m = 0.3491$, $m_g = B = 16$, $V = 24$, $r_h/r_t = 0.6$, and $\tilde{\omega} = 3\pi$. A gust upwash amplitude, $a^{(u)} = 1$, is imposed at the inlet of the computational domain and its radial component $\hat{u}_r = 0$. For the uniform flow, only one propagating acoustic mode $(-8, 0)$ exists, while two propagating modes $[(-8, 0), (-8, 1)]$ exist for the three swirling flows.

Figure 10 compares the magnitude of the unsteady sectional lift coefficient, $|c_l'|$, along the span for the different mean flows. The figure shows significant differences

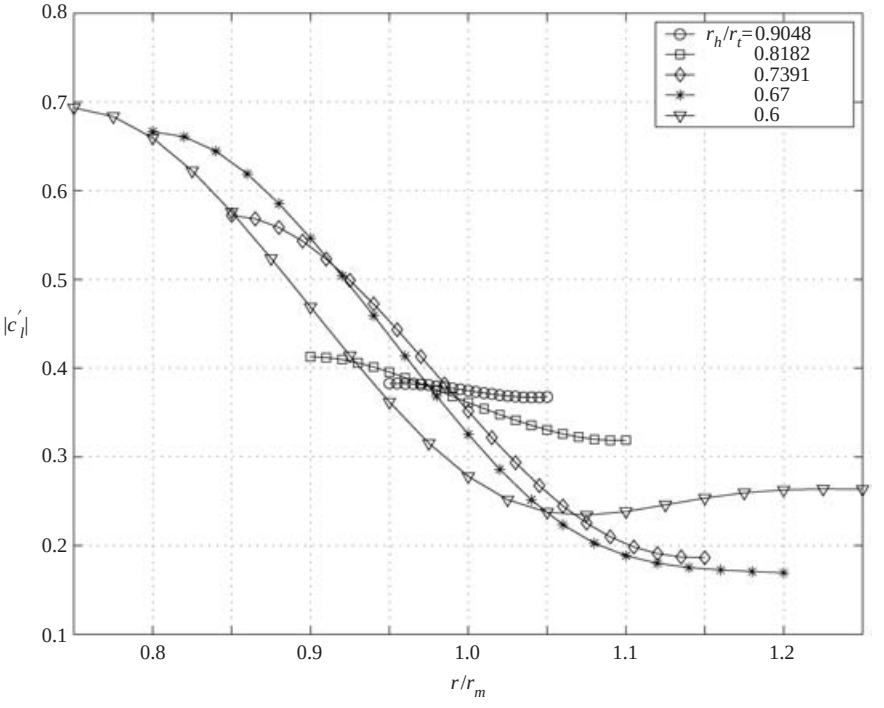

FIGURE 9. Variation of the magnitude of the unsteady sectional lift coefficient $|c_l'|$ along the span for different hub–tip ratios. A gust upwash amplitude, $a^{(u)} = 1$, is imposed at the vane leading edge. $M_0 = 0.3536$, $M_\Omega = 0.1$, $M_\Gamma = 0.1$, and $\tilde{\omega} = 3\pi$.

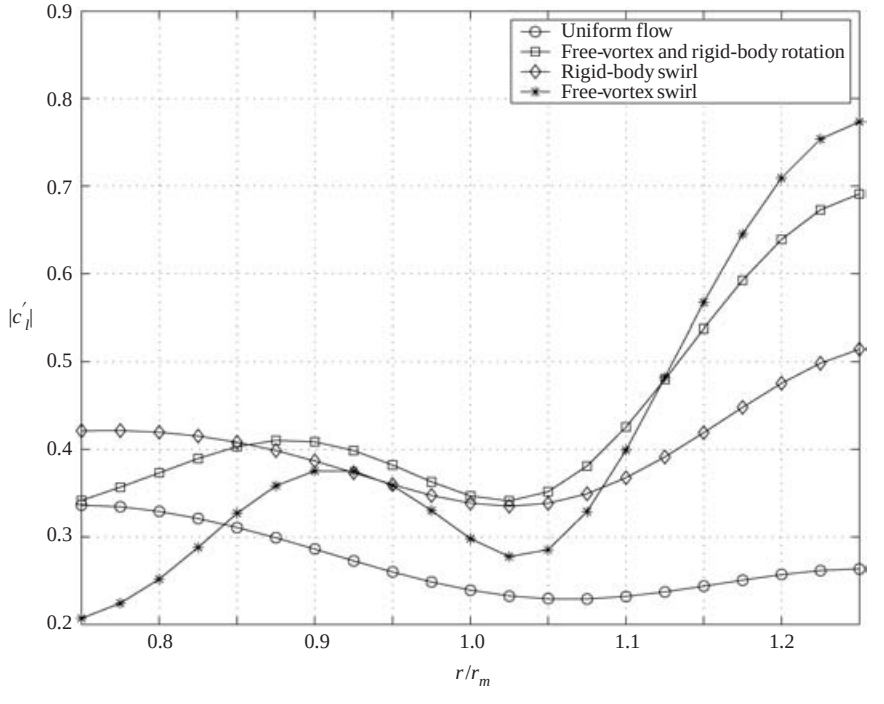

FIGURE 10. Variation of the magnitude of the unsteady sectional lift coefficient, $|c_l'|$, along the span for different mean flows. $r_h/r_t = 0.6$ and $\tilde{\omega} = 3\pi$.

	$M_0 = 0.4062$ $M_\Omega = 0$ $M_\Gamma = 0$	$M_0 = 0.3536$ $M_\Omega = 0$ $M_\Gamma = 0.2$	$M_0 = 0.3536$ $M_\Omega = 0.2$ $M_\Gamma = 0$	$M_0 = 0.3536$ $M_\Omega = 0.1$ $M_\Gamma = 0.1$
First downstream mode	0.1780	0.0935	0.1531	0.1380
Second downstream mode	Cut off	0.1686	0.1314	0.1492
First upstream mode	0.1590	0.0022	0.0100	0.0079
Second upstream mode	Cut off	0.0240	0.0674	0.0450

TABLE 2. Magnitude of the upstream and downstream acoustic coefficients, $|c_{mn}^{\pm}|$, for different mean flows. $r_h/r_t = 0.6$ and $\tilde{\omega} = 3\pi$.

between the various cases, with the free-vortex swirl showing the largest variation between hub and tip. The magnitude of the upstream and downstream acoustic coefficients, $|c_{mn}^{\pm}|$, are given in table 2. The table shows that for the three swirling flows the upstream acoustic coefficients are much smaller than that of the uniform flow, whereas the downstream coefficients are comparable to that of the uniform flow case. It is also interesting to note that for the swirling flows the downstream scattered energy is shared between the first and second acoustic modes, whereas most of the upstream scattered acoustic energy is contained in the second acoustic mode. We also note that for the free-vortex case a larger proportion of the scattered acoustic energy is in the second mode than for the combined swirl, which is larger than for the rigid-body swirl. In order to explain this result, we examine the incident-gust radial phase variation. For the rigid-body swirl, the gust phase at the midchord, $x = 0$, increases from hub to tip by about 0.9π, whereas it increases by 1.5π for the free-vortex case. Thus for the free-vortex swirl, the incident gust has a larger radial phase variation, which enhances its coupling with the second acoustic mode.

4.5. *Effects of incident disturbance coupling with duct modes on the scattering*

Often, the largest amplitudes of the incident vortical disturbance occur in the hub and/or tip regions of the duct where viscous effects and hub and tip vortices result in significant intensification of the wake. In what follows, we study how *hub-dominated* or *tip-dominated* vortical disturbances modify the scattering into sound. We also examine how the radial profile of the acoustic modes, which is independent of the incident-gust radial profile, affects scattering, particularly if they also are hub-dominated or tip-dominated. We recall that for a linear cascade the spanwise variation of the incident disturbances is exactly reproduced by the acoustic modes, indicating a total radial profile coupling between the noise source and the acoustic modes.

To this end, we consider the following two cases. In case 1, we impose at the inlet a hub-dominated incident vortical disturbance of the form

$$a_{m_g}^{(u)} = \cos\left(\frac{\pi}{2}\frac{r - r_h}{r_t - r_h}\right), \tag{4.11}$$

$$\hat{u}_{m_g r} = 0. \tag{4.12}$$

In case 2, we impose at the inlet a tip-dominated incident vortical disturbance of the form

$$a_{m_g}^{(u)} = \cos\left(\frac{\pi}{2}\frac{r_t - r}{r_t - r_h}\right), \tag{4.13}$$

$$\hat{u}_{m_g r} = 0. \tag{4.14}$$

		Case 1 Hub-dominated disturbance		Case 2 Tip-dominated disturbance	
	n	$\lvert c^{+}_{mn}\rvert$	$\lvert c^{-}_{mn}\rvert$	$\lvert c^{+}_{mn}\rvert$	$\lvert c^{-}_{mn}\rvert$
Uniform flow $M_0 = 0.4$, $M_\Omega = 0.$, $M_\Gamma = 0.$	1	0.048 (ht)	0.040 (ht)	0.059 (tt)	0.053 (tt)
	2	0.099 (hh)	0.073 (hh)	0.009 (th)	0.008 (th)
Rigid body swirl $M_0 = 0.34$, $M_\Omega = 0.2107$, $M_\Gamma = 0.$	1	0.083 (ht)	0.018 (hh)	0.102 (tt)	0.03 (th)
	2	0.110 (hh)	0.025 (hh)	0.020 (th)	0.049 (th)
Potential swirl $M_0 = 0.2828$, $M_\Gamma = 0.2828$, $M_\Omega = 0.$	1	0.018 (hh)	0.009 (hh)	0.038 (th)	0.016 (th)
	2	0.017 (hh)	0.006 (hh)	0.075 (th)	0.028 (th)

TABLE 3. Magnitude of the upstream and downstream acoustic modes, $|c^{\pm}_{mn}|$, for a uniform flow and hub-dominated and tip-dominated swirling mean flows, $\tilde{\omega} = 2.5\pi$. The first letter indicates whether the disturbance is hub-dominated (h) or tip-dominated (t). The second letter indicates whether the propagating mode is hub-dominated (h) or tip-dominated (t).

We take a stage defined by $B = 20$, $V = 24$, and $c/r_m = 0.2618$. The reduced frequency of the disturbance is 2.5π, $m_g = 20$ and $m = -4$. We consider three different mean flows: a uniform mean flow, a free-vortex swirling flow and a rigid-body swirling flow in a duct with hub–tip ratio of 0.5. The parameters of the mean flows and the magnitude of the downstream (+) and upstream (−) acoustic modes, $|c^{\pm}_{mn}|$, are given in table 3. There are two propagating acoustic modes for each case. The first downstream and upstream modes are plotted versus r in figures 11 and 12, respectively. Note that for the uniform flow and the rigid-body swirl, the first downstream mode is tip-dominated, i.e. the amplitude of the eigenfunctions approaches unity in the tip region and is less than one half in the hub region. For the potential swirling flow, the first mode is quite hub-dominated, i.e. both the upstream and downstream first radial mode amplitudes approach unity near the hub. On the other hand, the first upstream mode is only tip-dominated for the uniform flow and hub-dominated for the two other cases. For all flow cases considered, the second modes are hub-dominated.

Again, we examine the radial variation of the phase of the gust at the midchord, $x = 0$. For the rigid-body swirl, the gust phase increases from hub to tip by only 0.8π. As a result, these two cases allow us to examine how the scattering is modified by the change in the duct modes which results from the swirling flow. The free-vortex swirl case, in contrast, produces a significant tip to hub variation in the phase of the incident gust of about 3π. As will be seen below, this significantly reduces the generation of the scattered acoustic energy.

Table 3 shows the magnitude of the upstream and downstream acoustic modes for each case and for the different swirling flows. To facilitate the interpretation of the results, each case is denoted by two letters. The first letter indicates whether the disturbance is hub-dominated (h) or tip-dominated (t). The second letter indicates whether the propagating mode is hub-dominated (h) or tip-dominated (t). For the

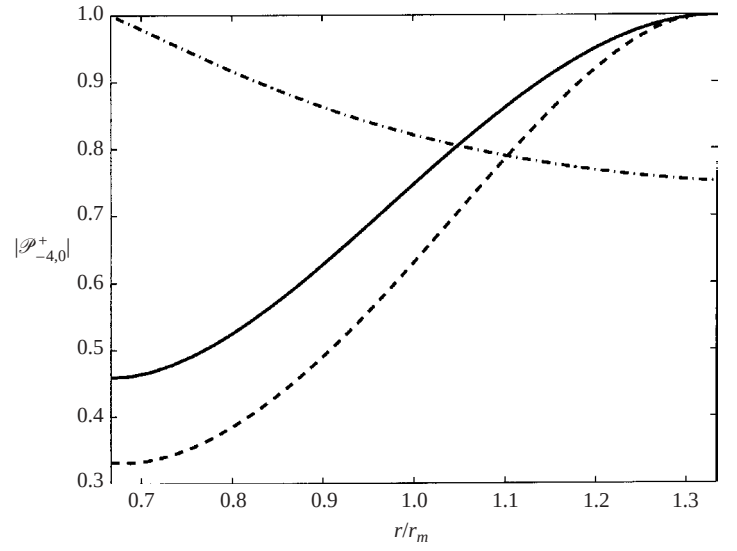

FIGURE 11. Radial variation of the magnitude of the first downstream acoustic mode, $|\mathscr{P}^{+}_{-4,0}|$, for a uniform flow (——), a rigid body swirl (– – –), and a free vortex swirl (— · —); $\tilde{\omega} = 2.5\pi$.

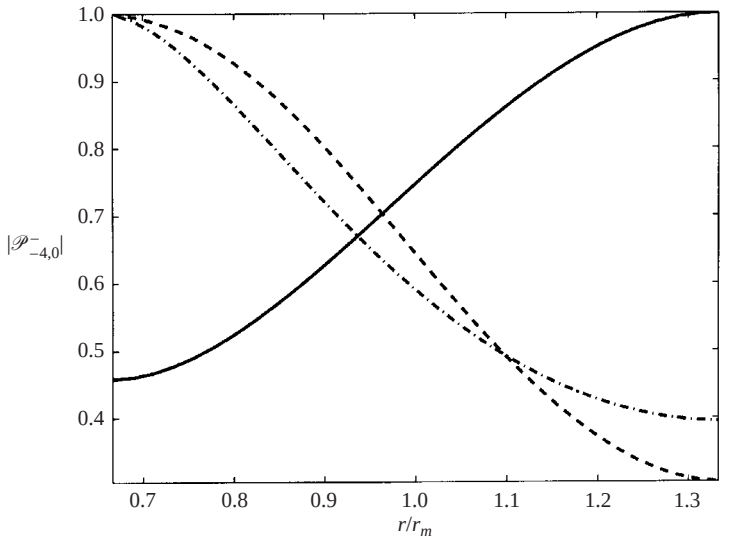

FIGURE 12. Radial variation of the magnitude of the first upstream acoustic mode, $|\mathscr{P}^{-}_{-4,0}|$, for a uniform flow (——), a rigid body swirl (– – –), and a free vortex swirl (— · —); $\tilde{\omega} = 2.5\pi$.

uniform flow and the rigid-body swirl, the scattered acoustic energy is largest for (hh) or (tt), suggesting that a hub-dominated (tip-dominated) disturbance will scatter more energy into a hub-dominated (tip-dominated) modes. Thus there is coupling between the noise source and the acoustic modes. This situation is reversed for the (ht) or (th) cases where the coupling is rather weak. Note also that when both modes are coupled or uncoupled the scattered acoustic energy is shared between the two modes. For the potential swirl, the incident-gust radial phase variation is large, resulting in

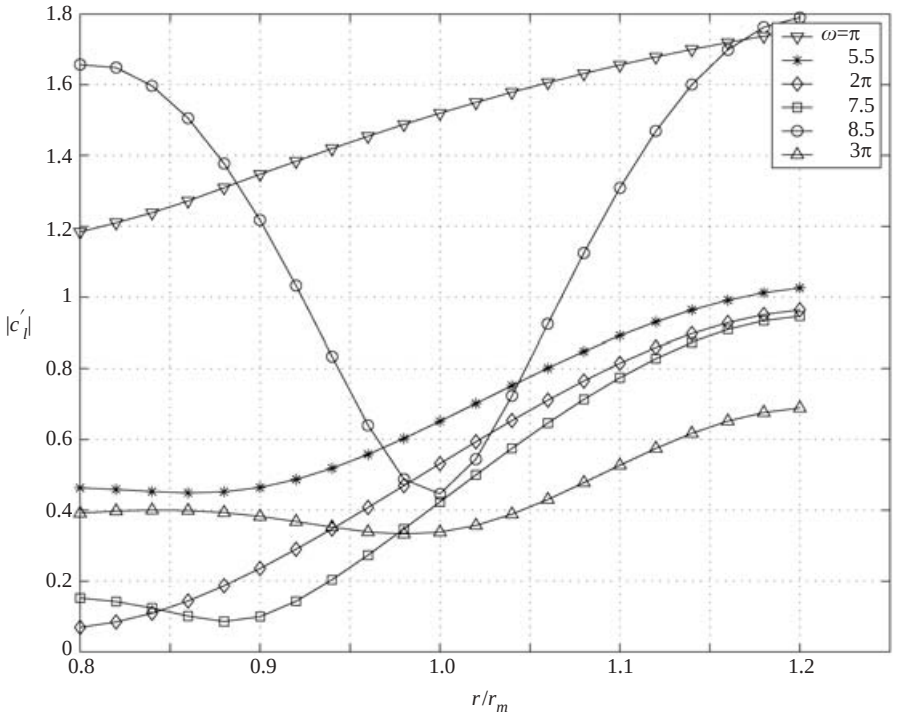

FIGURE 13. Variation of the magnitude of the unsteady sectional lift coefficient, $|c_l'|$, along the span for different reduced frequencies. $M_0 = 0.3536$, $M_\Omega = 0.1$, $M_\Gamma = 0.1$, and $r_h/r_t = 0.6667$.

weak coupling between the incident disturbances and the acoustic modes and leading to a reduced level of scattered acoustic energy.

Note that for a linear cascade, there is total radial profile coupling between the noise source and the acoustic modes. Thus the present results show an important characteristic of scattering by an annular cascade and the limitation of the linear cascade model.

4.6. *Modification of aeroacoustic response with reduced frequency*

In this subsection, we examine the unsteady sectional lift and acoustic coefficients for various reduced frequencies. The mean flow and geometric parameters are $M_0 = 0.3536$, $M_\Omega = 0.1$, and $M_\Gamma = 0.1$, $r_h/r_t = 0.6667$, $c/r_m = 0.3491$, $\tilde{\omega} = 3\pi$, $m_g = B = 16$, $V = 24$. A gust upwash amplitude, $a^{(u)} = 1$, with a radial component $\hat{u}_r = 0$ is imposed.

Figure 13 compares the magnitude of the unsteady sectional lift coefficient, $|c_l'|$, along the span for different values of the reduced frequency. The variation of the magnitude of the upstream and downstream acoustic coefficients, $|c^{\pm}_{-8,n}|$, versus the reduced frequency, $\tilde{\omega}$, are shown in figure 14. In order to explain the variation of $|c_l'|$ with the frequency, $\tilde{\omega}$, shown in figure 13, it is necessary to examine how the duct acoustics change with $\tilde{\omega}$.

Figure 13 shows that the values of $|c_l'|$ drop significantly as $\tilde{\omega}$ increases from π to 5.5, which is just below the first acoustic mode cut-on frequency of 6.07. As $\tilde{\omega}$ increases further, $|c_l'|$ generally continues to decrease. However, for $\tilde{\omega} = 8.5$, which close to the second acoustic mode cut-on frequency of 9.06, the radial distribution of $|c_l'|$ exhibits large variation from hub to tip. As the second acoustic mode cuts

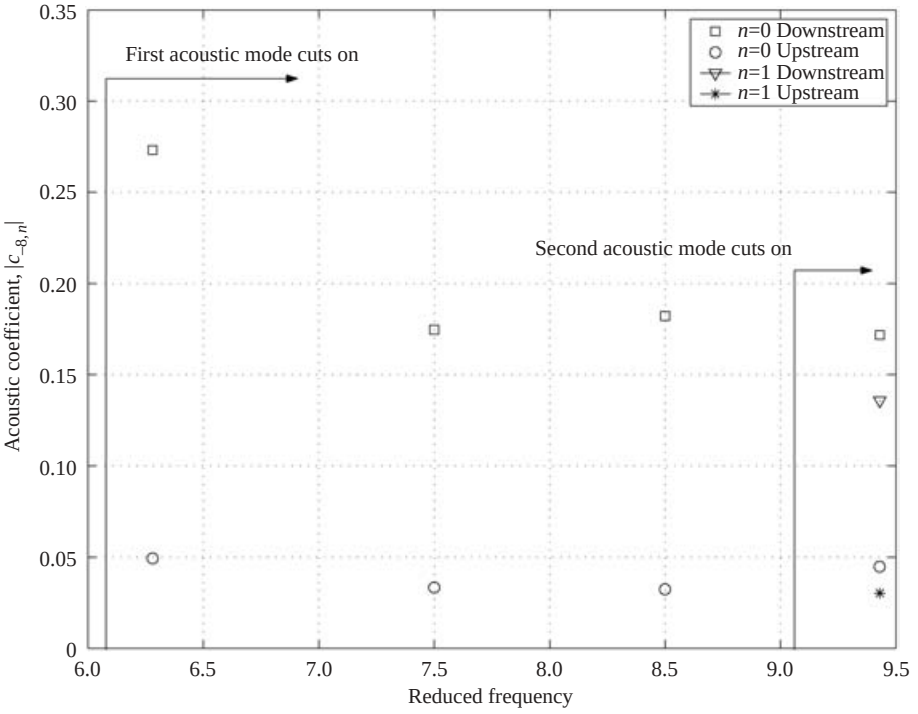

FIGURE 14. Variation of the magnitude of the upstream and downstream acoustic coefficients, $|c^{\pm}_{-8,n}|$, versus the reduced frequency. $M_0 = 0.3536$, $M_\Omega = 0.1$, $M_\Gamma = 0.1$ and $r_h/r_t = 0.6667$.

	2-D upstream disturbance	3-D upstream disturbance
First downstream mode	0.1359	0.1163
Second downstream mode	0.1718	0.1434
First upstream mode	0.0047	0.0039
Second upstream mode	0.0303	0.0273

TABLE 4. Magnitude of the upstream and downstream acoustic coefficients, $|c^{\pm}_{mn}|$ for two- and three-dimensional incident disturbances.

on, more acoustic energy propagates in the duct and for $\tilde{\omega} = 3\pi$, the magnitude and spanwise variation of $|c'_l|$ are greatly reduced.

4.7. *Effect of the radial velocity on the gust vane interaction*

To investigate the effect of the gust three-dimensionality, we consider two cases. In the first case, we have a two-dimensional gust with $\hat{u}_r = 0$ and in the second case, $\hat{u}_r = \sin(\pi(r - r_h)/(r_t - r_h))$. The mean flow and geometric parameters are $M_0 = 0.3536$, $M_\Omega = 0.1$, and $M_\Gamma = 0.1$, $r_h/r_t = 0.6667$, $c/r_m = 0.3491$, $\tilde{\omega} = 3\pi$, $B = 16$, $V = 24$.

Figure 15 compares the spanwise variation of the magnitude of the unsteady sectional lift coefficients for the two cases. When $\hat{u}_r = 0$, $|c'_l|$ is larger, especially near the tip. The magnitude of the upstream and downstream acoustic coefficients, $|c_{-8,n}|$, for the two cases are compared in table 4. Similarly to the lift coefficient, both the upstream and downstream modes are larger when $\hat{u}_r = 0$. This may occur because $\hat{u}_r$

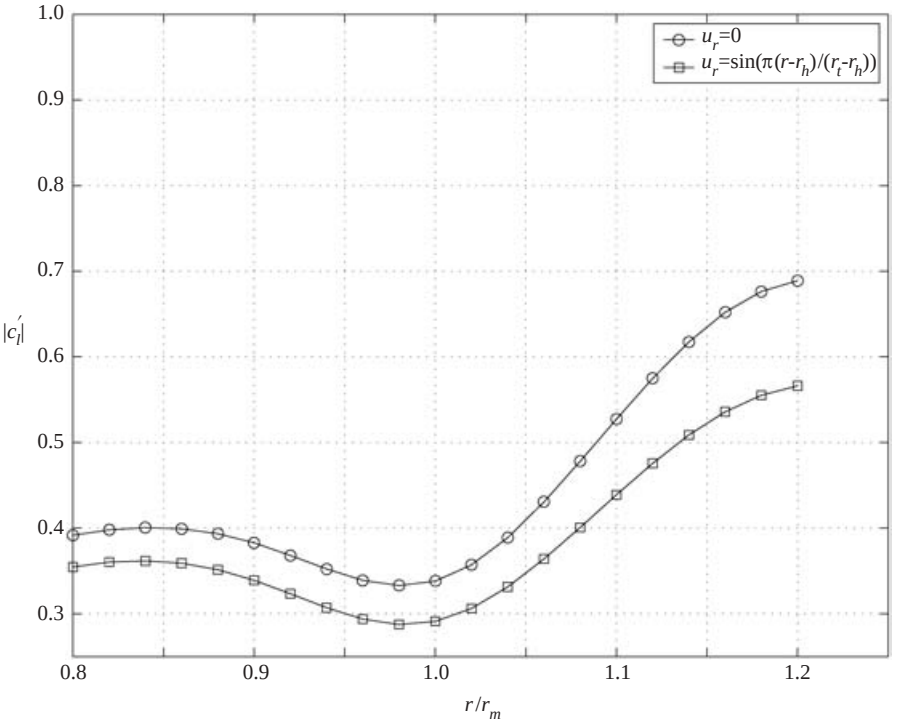

FIGURE 15. Variation of the magnitude of the unsteady sectional lift coefficient, $|c_l'|$, for two- and three-dimensional incident disturbances. $M_0 = 0.3536$, $M_\Omega = 0.1$, $M_\Gamma = 0.1$, $r_h/r_t = 0.6667$, and $\tilde{\omega} = 3\pi$.

affects the evolution of the other velocity components of the incident disturbance in the duct, which then changes the response by the usual momentum blocking.

4.8. *Sound transmission through a cascade*

We consider the scattering of an incident acoustic mode ($m = -8$, $n = 0$) by the annular cascade and compare the results with those of the scattering of a vortical disturbance. For comparison, we impose a unit upwash amplitude at the mean radius, $a_m^{(u)} = 1$, for both disturbances. For the incident acoustic mode the values of the upwash amplitude, $a_{-8,0}^{(u)}$, along the span are determined by the eigenfunction $\mathscr{P}_{-8,0}$, which varies slightly (about 10%). In order to impose a unit upwash amplitude at the mean radius, we take the incident acoustic mode coefficient defined by (4.8), $c_{-8,0}^{i} = 1.18$. For the vortical disturbance, we impose a constant amplitude upwash, $a_{m_g}^{(u)} = 1$, along the radius. The mean flow and geometric parameters for both cases are $M_0 = 0.3536$, $M_\Omega = 0.1$, $M_\Gamma = 0.1$, $r_h/r_t = 0.6667$, $c/r_m = 0.3491$ at the mean radius, $\tilde{\omega} = 3\pi$, and $\hat{u}_r = 0$.

Figure 16 compares the magnitude of the unsteady sectional lift coefficient along the span for the two cases. The lift coefficient is much larger for the acoustic disturbance. This may be explained by the fact that (i) the wavelength of the acoustic wave in the x-direction is much larger than that of the vortical wave, and (ii) the mean swirl changes the magnitude and phase of the vortical disturbance. These two effects cause phase cancellation along the blade in the case of the vortical disturbance, thus reducing the lift coefficient.

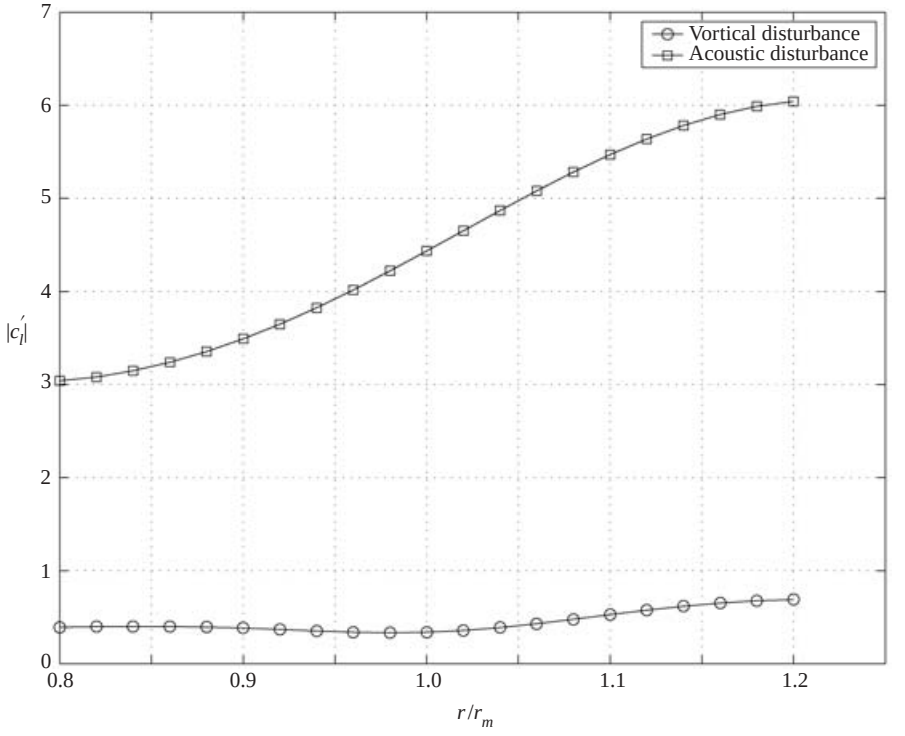

FIGURE 16. Comparison of the magnitude of the unsteady sectional lift coefficient, $|c_l'|$, along the span for acoustic and vortical incident disturbances. $M_o = 0.3536$, $M_\Omega = 0.1$, $M_\Gamma = 0.1$, $r_h/r_t = 0.6667$, and $\tilde{\omega} = 3\pi$.

	Vortical upstream disturbance	Acoustic upstream disturbance
First downstream mode	0.1359	0.8030
Second downstream mode	0.1718	0.5029
First upstream mode	0.0047	0.0154
Second upstream mode	0.0303	0.0526

TABLE 5. Magnitude of the upstream and downstream acoustic coefficients, $|c_{mn}^{\pm}|$ for acoustic and vortical incident disturbances.

The magnitude of the upstream and downstream acoustic coefficients, $|c_{-8,n}^{\pm}|$, for the two cases are compared in table 5. The acoustic coefficients are much larger in the case of the acoustic disturbance, especially for the first downstream acoustic mode. This is because the incident acoustic wave is the same as the first propagating duct mode and hence has an identical radial profile, supporting the analysis of the results of § 4.7. Comparing the upstream and downstream coefficients in the case of the acoustic disturbance, we see that most of the acoustic energy of the incident acoustic wave has been transmitted downstream and that the part that is reflected is relatively small.

5. Conclusions

The fundamental problem of scattering of vortical and acoustic waves by an annular blade cascade in a non-uniform flow is formulated. Numerical results are presented

to (i) examine and help us understand how swirl modifies the scattering compared to that of existing theories for the uniform flow limit and the narrow annulus limit, and (ii) determine what conditions lead to strong scattering of disturbances in the duct. Although the problem depends on many parameters, the results suggest that the swirl introduces additional non-uniformities which modify the physics of the scattering in three major ways: (i) it modifies the number of propagating acoustic modes in the duct, (ii) it changes their radial variation in the duct, and (iii) it causes significant amplitude and radial phase variation of the incident disturbances. Moreover, when the radial phase of the incident disturbance is different from the duct modes, weak scattering into the acoustic modes occurs. This occurs, for example, in a free-vortex swirling flow where large radial phase variations in the incident gust produce a weak coupling to the acoustic duct modes. Another way in which this can occur is when the incident vortical wave is tip-dominated and the propagating acoustic modes are hub-dominated. These results suggest that analysis of the radial variation of the incident disturbance and duct modes can provide an indication of the efficiency of the scattering process. It also explains why the scattering of a downstream incident acoustic wave into downstream acoustic energy is more efficient than that of an incident vortical wave.

This research was supported by the Office of Naval Research grant No. N00014-00-1-0130 with Dr Ki-Han Kim as program manager, and the Ohio Aerospace Institute Aeroacoustic Consortium. The authors would like to thank Dr Basman Elhadidi for his help in the computations.

Appendix. The velocity of a normal mode in terms of the pressure

In a normal-mode analysis of an isentropic flow, the flow quantities can be expressed, as in equation (3.3), in terms of the normal modes

$$\{p'^{\pm}, u_x^{\pm}, u_r^{\pm}, u_\theta^{\pm}\}(x, r, \theta; t) = \int_{-\infty}^{+\infty} \sum_{n=0}^{\infty} \sum_{m \in S_m^{\pm}} c_{mn}^{\pm} \{\mathscr{P}_{mn}^{\pm}(r), u_{x\,mn}^{\pm}(r), u_{r\,mn}^{\pm}(r), u_{\theta\,mn}^{\pm}(r)\} \times \mathrm{e}^{\mathrm{i}(k_{mn}x + m\theta - \omega t)}\, \mathrm{d}\omega. \quad (A\,1)$$

Substituting (A 1) into the linearized Euler equations and dropping the $\pm$ sign, gives for every $\{mn\}$ mode,

$$\Lambda_{mn} u_{x\,mn} - \frac{\mathrm{d}U_x}{\mathrm{d}r}(\mathrm{i}u_{r\,mn}) = -\frac{k_{mn}}{\rho_0}\mathscr{P}_{mn}, \quad (A\,2)$$

$$\Lambda_{mn} u_{\theta\,mn} - \frac{1}{r}\frac{\mathrm{d}(rU_\theta)}{\mathrm{d}r}(\mathrm{i}u_{r\,mn}) = -\frac{m}{r\rho_0}\mathscr{P}_{mn}, \quad (A\,3)$$

$$\Lambda_{mn}(\mathrm{i}u_{r\,mn}) - \frac{2U_\theta}{r}u_{\theta\,mn} = -\frac{1}{\rho_0}\frac{\mathrm{d}\mathscr{P}_{mn}}{\mathrm{d}r} + \frac{U_\theta^2}{c_0^2 r\rho_0}\mathscr{P}_{mn}, \quad (A\,4)$$

where

$$\Lambda_{mn} = -\omega + k_{mn}U_x + \frac{mU_\theta}{r}. \quad (A\,5)$$

Using equations (A 2), (A 3), (A 4), the eigenfunctions for the velocity $\{u_{xmn}, u_{rmn}, u_{\theta mn}\}$ can be expressed in terms of that of the pressure $\mathscr{P}_{mn}$,

$$u_{xmn} = \left(\frac{\dfrac{\mathrm{d}U_x}{\mathrm{d}r}\left(\dfrac{U_\theta^2}{c_0^2 r\rho_0} - \dfrac{2mU_\theta}{r^2\rho_0\Lambda_{mn}}\right)}{\Lambda_{mn}^2 - \dfrac{2U_\theta}{r^2}\dfrac{\mathrm{d}}{\mathrm{d}r}(rU_\theta)} - \frac{k_{mn}}{\rho_0\Lambda_{mn}} \right)\mathscr{P}_{mn} - \frac{\dfrac{\mathrm{d}U_x}{\mathrm{d}r}}{\rho_0\left(\Lambda_{mn}^2 - \dfrac{2U_\theta}{r^2}\dfrac{\mathrm{d}}{\mathrm{d}r}(rU_\theta)\right)}\frac{\mathrm{d}\mathscr{P}_{mn}}{\mathrm{d}r}, \tag{A 6}$$

$$u_{rmn} = \frac{-\mathrm{i}}{\Lambda_{mn}^2 - \dfrac{2U_\theta}{r^2}\dfrac{\mathrm{d}}{\mathrm{d}r}(rU_\theta)}\left(\left(\frac{U_\theta^2\Lambda_{mn}}{c_0^2 r\rho_0} - \frac{2mU_\theta}{r^2\rho_0}\right)\mathscr{P}_{mn} - \frac{\Lambda_{mn}}{\rho_0}\frac{\mathrm{d}\mathscr{P}_{mn}}{\mathrm{d}r}\right), \tag{A 7}$$

$$u_{\theta mn} = \frac{1}{\Lambda_{mn}^2 - \dfrac{2U_\theta}{r^2}\dfrac{\mathrm{d}}{\mathrm{d}r}(rU_\theta)}\left(\left(\frac{U_\theta^2}{c_0^2 r^2\rho_0}\frac{\mathrm{d}}{\mathrm{d}r}(rU_\theta) - \frac{m\Lambda_{mn}}{r\rho_0}\right)\mathscr{P}_{mn} - \frac{1}{r\rho_0}\frac{\mathrm{d}}{\mathrm{d}r}(rU_\theta)\frac{\mathrm{d}\mathscr{P}_{mn}}{\mathrm{d}r}\right). \tag{A 8}$$

REFERENCES

Ali, A. A. 2001 Aeroacoustics and stability of swirling flow. PhD thesis, University of Notre Dame.

Ali, A. A., Atassi, O. V. & Atassi, H. M. 2000 Acoustic eigenmodes in a coannular duct with a general swirling flow. *AIAA Paper* 2000-1954.

Ali, A. A., Atassi, O. V. & Atassi, H. M. 2001 Derivation and implementation of inflow/outflow conditions for aeroacoustic problems with swirling flows. In *AIAA Paper* 2001-2173.

Atassi, H. M. 1994 Unsteady aerodynamics of vortical flows: early and recent developments. In *Aerodynamics and Aeroacoustics* (ed. K.-Y. Fung), pp. 121–172. World Scientific.

Atassi, H. M. & Grzedzinski, J. 1989 Unsteady disturbances of streaming motions around bodies. *J. Fluid Mech.* **209**, 385–403.

Atassi, H. M. & Hamad, G. 1981 Sound generation in a cascade by 3D disturbance convected in a subsonic flow. In *AIAA Paper* 81-2046.

Atassi, O. V. & Ali, A. A. 2002 Inflow/outflow conditions for time-harmonic internal aeroacoustic problems. *J. Comput. Acoust.* **10**, 155–182.

Briggs, R. 1964 *Electron-Stream Interaction with Plasmas*. The MIT Press.

Elhadidi, B. M., Atassi, H. M., Envia, E. & Podboy, G. 2000 Evolution of rotor wake in swirling flow. *AIAA Paper* 2000-1991.

Fang, J. & Atassi, H. 1993 Compressible flows with vortical disturbances around a cascade of loaded airfoils. In *Unsteady Aerodynamics, Aeroacoustics, and Aeroelasticity of Turbomachines and Propellers* (ed. H. M. Atassi), pp. 149–176. Springer.

Glegg, S. A. L. 1999 The response of a swept blade row to a three dimensional gust. *J. Sound Vib.* **227**, 29–64.

Goldstein, M. E. 1976 *Aeroacoustics*. McGraw-Hill.

Goldstein, M. E. 1978 Unsteady vortical and entropic distortions of potential flows round arbitrary obstacles. *J. Fluid Mech.* **89**, 433–468.

Goldstein, M. E. & Atassi, H. M. 1976 A complete second-order theory for the unsteady flow about an airfoil due to a periodic gust. *J. Fluid Mech.* **74**, 741–765.

Golubev, V. V. & Atassi, H. M. 1998 Acoustic-vorticity waves in swirling flows. *J. Sound Vib.* **209**, 203–222.

Golubev, V. V. & Atassi, H. M. 2000*a* Interaction of unsteady swirling flows with annular cascades. Part II. aerodynamic blade response. *AIAA J.* **38**, 1150–1157.

Golubev, V. V. & Atassi, H. M. 2000*b* Unsteady swirling flows in annular cascades. part I. evolution of incident disturbances. *AIAA J.* **38**, 1142–1149.

Hall, K. C. & Verdon, J. M. 1991 Gust response analysis for cascades operating in nonuniform mean flows. *AIAA J.* **29**, 1463–1471.

Hanson, D. B. 1999 Fan stator with harmonic excitation by rotor wake. *Third CAA Workshop on Benchmark Problems*, Category 4.

Kaji, S. & Okazaki, T. 1970*a* Generation of sound by rotor-stator interaction. *J. Sound Vib.* **13**, 281–307.

Kaji, S. & Okazaki, T. 1970*b* Propagation of sound waves through a blade row. II. Analysis based on the acceleration potential method. *J. Sound Vib.* **11**, 355–375.

Kerrobrock, J. L. 1977 Small disturbances in turbomachine annuli with swirl. *AIAA J.* **15**, 794–803.

Kovasznay, L. S. 1953 Turbulence in supersonic flow. *J. Aero. Sci.* **20**, 657–674.

Montgomery, M. D. & Verdon, J. M. 1997 A three-dimensional linearized unsteady Euler analysis for turbomachinery blade rows. *NASA CR*-4770.

Namba, M. 1987 Three-dimensional flow. In *Unsteady Turbomachinery Aerodynamics, AGARD*-AG-298.

Namba, M. & Schulten, J. B. H. M. 2000 Category 4-fan stator with harmonic excitation by rotor wake. *NASA/CP*-2000-209790.

Peake, N. & Kerschen, E. J. 1995 A uniform asymptotic approximation for high-frequency unsteady cascade flow. *Proc. R. Soc. Lond.* A **449**, 177–186.

Podboy, G. G., Krupar, M. J., Christopher, E. H. & Richard, P. W. 2002 Fan noise source diagnostic test-ldv measured flow field results. In *AIAA Paper* 2002-2431.

Schulten, J. B. H. M. 1982 Sound generated by rotor wakes interacting with a leaned vane stator. *AIAA J.* **20**, 1352–1358.

Scott, J. R. & Atassi, H. M. 1995 A finite-difference frequency domain numerical scheme for the solution of the gust response problem. *J. Comput. Phys.* **119**, 75–93.

Smith, S. N. 1971 Discrete frequency sound generation in axial flows of turbomachines. *CUED*/A-Turbo/TR29.

Tyler, J. M. & Sofrin, T. G. 1962 Axial flow compressor noise studies. *SAE Trans.* **70**, 309–332.